The Plant Cell, Vol. 20: 2661–2680, October 2008, www.plantcell.org

IMPa-4, an *Arabidopsis* Importin α Isoform, Is Preferentially Involved in *Agrobacterium*-Mediated Plant Transformation [W]

Saikat Bhattacharjee,[1] Lan-Ying Lee, Heiko Oltmanns,[2] Hongbin Cao,[3] Veena,[4] Joshua Cuperus,[5] and Stanton B. Gelvin[6]

Department of Biological Sciences, Purdue University, West Lafayette, Indiana 47907

Successful transformation of plants by *Agrobacterium tumefaciens* requires that the bacterial T-complex actively escorts T-DNA into the host's nucleus. VirD2 and VirE2 are virulence proteins on the T-complex that have plant-functional nuclear localization signal sequences that may recruit importin α proteins of the plant for nuclear import. In this study, we evaluated the involvement of seven of the nine members of the *Arabidopsis thaliana* importin α family in *Agrobacterium* transformation. Yeast two-hybrid, plant bimolecular fluorescence complementation, and in vitro protein–protein interaction assays demonstrated that all tested *Arabidopsis* importin α members can interact with VirD2 and VirE2. However, only disruption of the importin *IMPa-4* inhibited transformation and produced the rat (resistant to *Agrobacterium* transformation) phenotype. Overexpression of six importin α members, including IMPa-4, rescued the rat phenotype in the *impa-4* mutant background. Roots of wild-type and *impa-4 Arabidopsis* plants expressing yellow fluorescent protein–VirD2 displayed nuclear localization of the fusion protein, indicating that nuclear import of VirD2 is not affected in the *impa-4* mutant. Somewhat surprisingly, VirE2–yellow fluorescent protein mainly localized to the cytoplasm of both wild-type and *impa-4 Arabidopsis* cells and to the cytoplasm of wild-type tobacco (*Nicotiana tabacum*) cells. However, bimolecular fluorescence complementation assays indicated that VirE2 could localize to the nucleus when IMPa-4, but not when IMPa-1, was overexpressed.

INTRODUCTION

The Gram-negative soil bacterium *Agrobacterium tumefaciens* is the causative agent of crown gall tumors in plants. Plant transformation results from interkingdom transfer of genetic material from bacteria to plant cells and is the end product of multiple events initiating in the bacterium and terminating in the infected plant (reviewed in Gelvin, 2000, 2003; Zupan et al., 2000; Tzfira and Citovsky, 2001; Lacroix et al., 2006; McCullen and Binns, 2006). During transformation, T-DNA, a part of the bacterial Ti-plasmid, is transferred from the bacterium to the plant cell with the aid of a number of Virulence (Vir) proteins encoded by the Ti-plasmid. Processing of T-DNA is initiated by the border-specific VirD1/VirD2 endonuclease (Yanofsky et al., 1986; Jayaswal et al., 1987; Filichkin and Gelvin, 1993), which nicks the bottom strand of T-DNA at T-DNA borders (Stachel et al., 1986; Wang et al., 1987). Nicking at border sequences is coupled to covalent linkage of VirD2 via its Tyr-29 residue to the 5′ end of the resulting single-stranded (ss) T-DNA molecule (Vogel and Das, 1992), the T-strand (Herrera-Estrella et al., 1988; Ward and Barnes, 1988; Durrenberger et al., 1989). VirE2, a nonspecific ssDNA binding (SSB) protein, cooperatively binds to the T-strand and protects it from endonucleases and exonucleases (Citovsky et al., 1989; Sen et al., 1989). The T-strand, with a single affixed VirD2 and coated with VirE2, is called the T-complex. Formation of the T-complex most likely occurs within the plant because T-strands and VirE2 proteins are transferred independently to plant cells (Otten et al., 1984; Citovsky et al., 1992; Binns et al., 1995; Stahl et al., 1998, Lee et al., 1999). A currently popular model posits that the assembled T-complex translocates to the nucleus, where T-DNA subsequently integrates into the plant genome.

In eukaryotes, the nuclear membrane separates the major genome from the rest of the cell. The double membrane nuclear envelope maintains structural integrity of the nucleus and allows molecular communication through specific channels, the nuclear pores, which contain proteins that form the nuclear pore complex. These channels serve as conduits for the passive diffusion of small macromolecules (<40 to 60 kD), metabolites, and ions. By contrast, nuclear translocation of most macromolecules requires an energy-dependent active import/export process (reviewed in Stewart et al., 2007), which is mediated by a variety of soluble nuclear transport factors. Many karyophilic proteins contain *cis*-acting nuclear localization signal (NLS) sequences that are recognized by these nuclear transport factors (Goldfarb et al., 2004).

Import of a NLS-containing protein is initiated by the energy-independent formation of a cargo-receptor complex, the nuclear pore-targeting complex (PTAC) (Quimby and Corbett, 2001; reviewed in Gasiorowski and Dean, 2003). PTAC contains two

[1] Current address: College of Agriculture, Food, and Natural Resources, University of Missouri–Columbia, Columbia, MO 65211.
[2] Current address: Kirchstrasse 30, 69221 Dossenheim, Germany.
[3] Current address: Department of Radiation Oncology, Stanford University, 269 Campus Drive, Stanford, CA 94305.
[4] Current address: Monsanto Company, 700 Chesterfield Parkway, St. Louis, MO 63017.
[5] Current address: Molecular and Cellular Biology Program, Oregon State University, Corvallis, OR 97331.
[6] Address correspondence to gelvin@bilbo.bio.purdue.edu.
The author responsible for distribution of materials integral to the findings presented in this article in accordance with the policy described in the Instructions for Authors (www.plantcell.org) is: Stanton B. Gelvin (gelvin@bilbo.bio.purdue.edu).
[W] Online version contains Web-only data.
www.plantcell.org/cgi/doi/10.1105/tpc.108.060467

factors, importin α and importin β. Importin α acts as an adaptor by recognizing the NLS cargo and then binds to importin β. Importin β is the carrier component of PTAC and targets the complex to the nuclear pore by binding to nuclear pore proteins collectively termed nucleoporins (Görlich et al., 1995; Bednenko et al., 2003). Once translocated to the nucleus, the complex is disassembled and importin α and importin β are recycled back to the cytoplasm (for a recent review of nucleocytoplasmic transport, see Terry et al., 2007).

Because any piece of DNA placed between T-DNA borders can be translocated from *Agrobacterium* into plant nuclei, information directing nuclear import of the T-complex must reside in the accompanying protein constituents, including VirD2 and VirE2. Both proteins can be imported into plant nuclei (Herrera-Estrella et al., 1990; Howard et al., 1992; Tinland et al., 1992; Citovsky et al., 1994; Mysore et al., 1998; Ziemienowicz et al., 2001). In VirD2, a highly conserved single cluster of four amino acids at the N terminus (R-K-G-K) and two short stretches of four to five residues at the C terminus resemble prototypic monopartite and bipartite NLSs, respectively. The close proximity of the N-terminal NLS to Tyr-29, to which T-DNA links (Vogel and Das, 1992), is likely to mask its in vivo nuclear import function. In isolation from the rest of the VirD2 protein, the C-terminal bipartite NLS can direct reporter protein fusions to plant, yeast, and animal nuclei (Howard et al., 1992; Shurvinton et al., 1992; Tinland et al., 1992; Rossi et al., 1993; Citovsky et al., 1994; Guralnick et al., 1996; Mysore et al., 1998).

VirE2 contains two central bipartite NLSs. Each of these can direct reporter protein fusions into plant nuclei individually, but efficient nuclear import requires both (Citovsky et al., 1992, 1994). Zupan et al. (1996) reported the nuclear localization of VirE2 complexed with ssDNA in microinjected plant cells. However, Ziemienowicz et al. (2001) claimed that nuclear import of large oligonucleotides in permeabilized plant cells required both VirE2 and VirD2 activity. Because the ssDNA binding and NLS domains of VirE2 overlap, VirE2 complexed with T-DNA may be unable to function in nuclear import of the T-complex (Citovsky et al., 1992; Ziemienowicz et al., 2001). At present, whether both VirD2 and VirE2 are required for nuclear import of the T-complex remains controversial.

Several studies have suggested the involvement of importin α in *Agrobacterium*-mediated transformation. Nuclear import of VirD2 and VirE2 proteins, and of synthetically generated T-complexes, can be inhibited by nonhydrolyzable GTP analogs (Zupan et al., 1996; Ziemienowicz et al., 2001), suggesting use of the importin pathway. Ballas and Citovsky (1997) and Bako et al. (2003) identified three *Arabidopsis thaliana* importin α members that interact with VirD2 in yeast. Because importin α is encoded by a multigene family in *Arabidopsis*, it is not clear whether multiple importin α isoforms or a specific importin α isoform is required for *Agrobacterium*-mediated transformation. Ballas and Citovsky (1997), however, were unable to demonstrate the interaction of VirE2 with *Arabidopsis* KAPα (also known as At KAPα; Ballas and Citovsky, 1997) in yeast. Rather, Tzfira et al. (2001) suggested that nuclear import of VirE2 is mediated through VIP1 (for VirE2-Interacting Protein1), an *Arabidopsis* protein belonging to a basic Leu zipper family. These authors showed that transgenic tobacco (*Nicotiana tabacum*) plants that express a *VIP1* antisense gene are recalcitrant to transformation, possibly because of a deficiency in nuclear targeting of VirE2 but not of VirD2. Li et al. (2005) further showed the importance of VIP1 in T-DNA integration as well as nuclear import.

In this study, we investigated the role of seven *Arabidopsis* importin α isoforms in *Agrobacterium*-mediated transformation. Using yeast two-hybrid analysis, plant bimolecular fluorescence complementation (BiFC), and in vitro interaction assays, we show that multiple importin α isoforms can interact not only with VirD2 but also with VirE2. However, only mutation of *IMPa4*, but not of the other importin α genes investigated, resulted in a transformation deficiency of the mutant plants.

RESULTS

Multiple *Arabidopsis* Importin α Isoforms Interact with VirD2 and VirE2

The *Arabidopsis* genome contains nine genes that encode importin α proteins (Figure 1; see Supplemental Data Set 1 online). We initially utilized a yeast two-hybrid approach to investigate the interaction of four of these importin α isoforms (KAPα [IMPa-1], IMPa-2, IMPa-3, and IMPa-4) (Figure 1; see Supplemental Figure 1 online) with VirD2 and VirE2. In these assays, the prey plasmid pGAD424 expressed either VirD2 or VirE2 as a translational fusion with the Gal4 activation domain. Correspondingly, the bait plasmid pSTT91 expressed importin α isoforms 1 to 4 as translational fusions with the LexA DNA binding domain. β-Galactosidase activity in these yeast strains was quantified using *o*-nitrophenyl β-D-galactoside (ONPG) assays. All four importin α isoforms tested interacted with both VirD2 and VirE2 (Figures 2A and 2C).

In vitro glutathione-*S*-transferase (GST) pull-down assays further demonstrated direct protein–protein interactions of KAPα, IMPa-2, IMPa-3, and IMPa-4 with both VirD2 and VirE2 (Figures 2B and 2D). Our VirD2 interaction results confirm and extend earlier reports of Ballas and Citovsky (1997) and Bako et al. (2003) with regard to KAPα and IMPa-3/IMPa-4 interaction with VirD2, respectively. Our results further indicate that multiple *Arabidopsis* importin α isoforms can recognize VirE2, an interaction not detected by Ballas and Citovsky (1997).

Mapping VirD2 and VirE2 Domains Important for Interaction with Importin α

VirD2 has monopartite- and bipartite-type NLSs located in the N-terminal and C-terminal regions of the protein, respectively (Figure 3A) (Herrera-Estrella et al., 1990; Howard et al., 1992; Shurvinton et al., 1992; Tinland et al., 1992; Rossi et al., 1993; Mysore et al., 1998). VirE2 has two central bipartite NLSs (NLS1 and NLS2) (Citovsky et al., 1992; Dombek and Ream, 1997) (Figure 3C). We generated a series of VirD2 and VirE2 deletion mutants (Figures 3A and 3C) and tested their interaction with IMPa-4 in yeast (Figures 3B and 3D). We found that a 46–amino acid domain located between the two C-terminal *Nru*I sites (R-372 to R-417) of VirD2 is important for interaction with IMPa-4 (Figure 3B). This domain of VirD2 includes the C-terminal

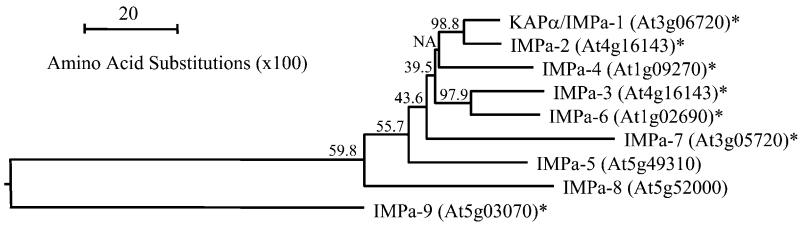

Figure 1. Cladogram of the Nine Importin α Proteins Investigated in This Study.

The genes encoding the corresponding importin α proteins are indicated in parentheses. Alignments were performed using ClustalW. The alignment information was used to generate a cladogram using MegAlign 7.1 (DNASTAR) and a bootstrap value of 1000, with seed of 111. Asterisks denote the importin α isoforms investigated in this study. Sequences used to generate the cladogram are presented in Supplemental Data Set 1 online.

bipartite-type NLS (KRPR-[X]$_9$-RKRAR). Interestingly, the mutant VirD2 fusion protein containing a precise deletion of the bipartite NLS residues (VirD2ΔNLS) also interacted with IMPa-4, albeit at a slightly lower strength (as indicated by units of β-galactosidase activity) than did the full-length VirD2 prey fusion (Figure 3B).

Interaction assays of IMPa-4 with the various VirE2 deletion proteins indicated that VirE2 interacts in yeast with IMPa-4 in a NLS dose-dependent manner. Yeast strains expressing the IMPa-4 bait fusion protein showed higher β-galactosidase activity with a truncated VirE2 protein containing both NLSs (N-ter 2-349) than with a mutant VirE2 protein containing only NLS1 (N-ter 2-242; Figure 3D). Surprisingly, a C-terminal 158–amino acid domain of VirE2 also interacted with IMPa-4 (Figure 3D). This domain of VirE2 does not contain any signature NLS sequence and overlaps with the ssDNA binding domain of VirE2.

We also performed in vitro pull-down assays using full-length and various deletion derivatives of VirD2 and VirE2 expressed as GST fusions and T7 epitope-tagged IMPa-4 (see Supplemental Figure 2 online). These assays further supported the observations obtained using yeast two-hybrid assays. Taken together, these data indicate that for both VirD2 and VirE2, the IMPa-4–interacting domains include but are not restricted to previously identified NLS residues (Citovsky et al., 1992; Howard et al., 1992).

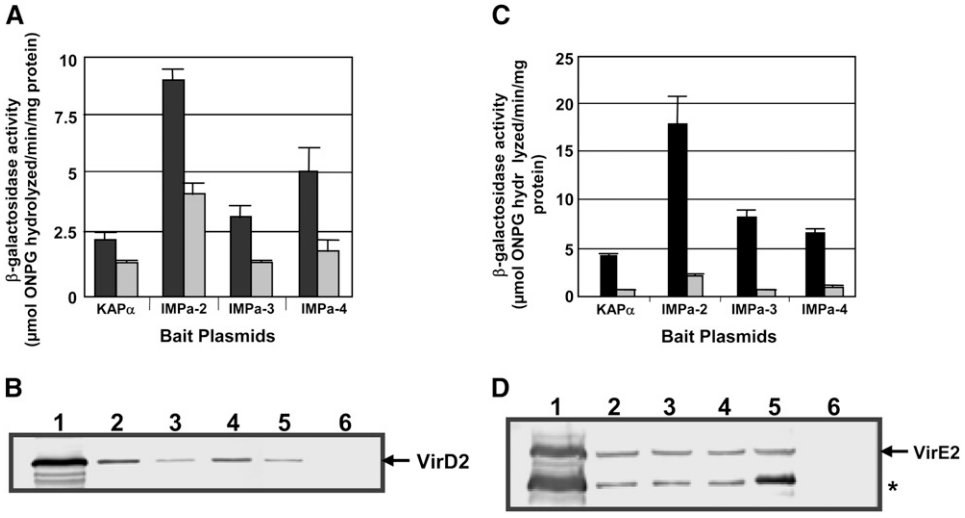

Figure 2. KAPα, IMPa-2, IMPa-3, and IMPa-4 Interact with VirE2 and VirD2.

(A) and **(C)** In yeast two-hybrid assays, yeast strains containing various bait/prey combinations were tested for *LacZ* activity using liquid ONPG as a β-galactosidase substrate. The black bars indicate *LacZ* activity in yeast strains containing importin α bait/VirD2 prey **(A)** or importin α bait/VirE2 prey **(C)** combinations. The gray bars show the *LacZ* activity in the yeast strains containing importin α bait/nonspecific GTPase prey. Error bars represent SE obtained with three biological replicates.

(B) and **(D)** KAPα, IMPa-2, IMPa-3, and IMPa-4 bind to VirD2 and VirE2 in vitro. GST-tagged importin α proteins and GST alone were linked to separate glutathione–Sepharose columns and treated with lysates from *E. coli* expressing VirD2 **(B)** or VirE2 **(D)**. Bound proteins were eluted, and equimolar fraction volumes were analyzed by immunoblot using either rabbit anti-octopine VirD2 **(B)** or anti-nopaline VirE2 **(D)** polyclonal antiserum as the primary antibody (1:1000 dilution) and goat anti-rabbit IgG conjugated to horseradish peroxidase as the secondary antibody (1:1000 dilution). Lane 1, VirD2 **(B)** or VirE2 **(D)** crude lysate. Lanes 2 to 6, eluted fractions from different columns: lane 2, GST-KAPα; lane 3, GST-IMPa-2; lane 4, GST-IMPa-3; lane 5, GST-IMPa-4; lane 6, GST. The asterisk represents a lower molecular weight, partially degraded VirE2 protein previously reported in the lysates of VirE2-expressing *E. coli* cells (Dombek and Ream, 1997).

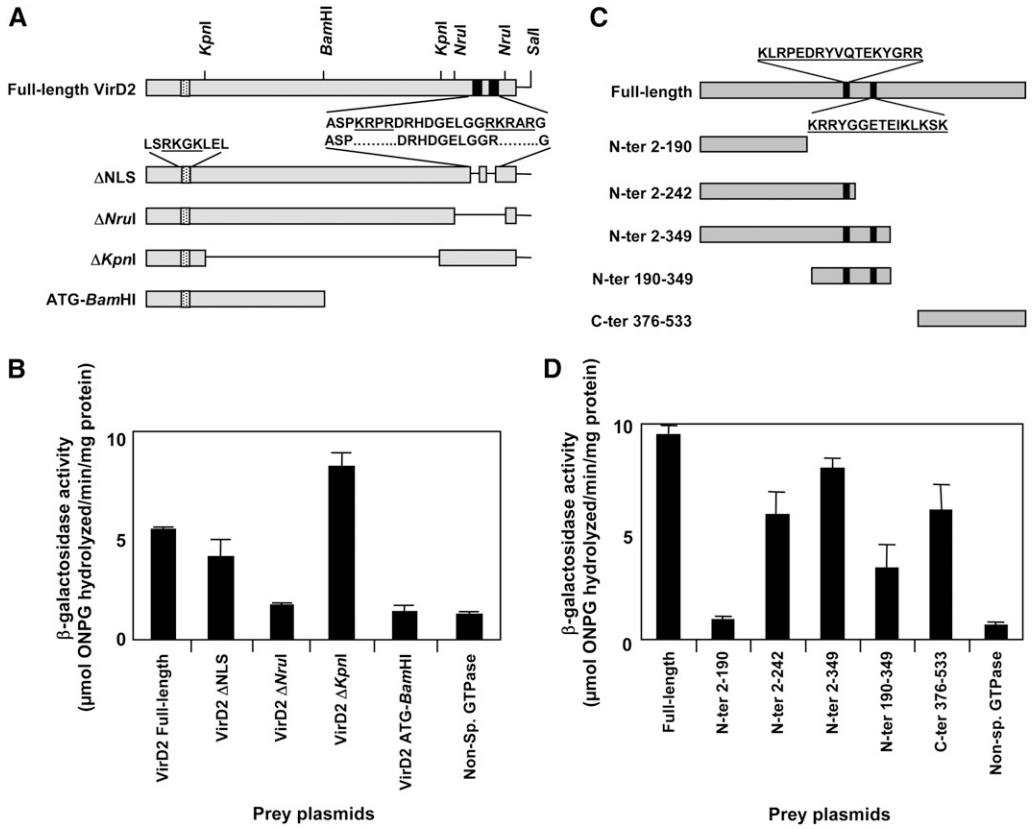

Figure 3. IMPa-4–Interacting Domains of VirD2 and VirE2.

(A) Schematic representation of the various VirD2 deletion mutants used. VirD2 protein or its truncated derivatives are shown as gray boxes. VirD2 contains two NLS, a N-terminal monopartite NLS (stippled box) and a C-terminal bipartite NLS (black boxes). Thin lines indicate deleted regions. The N- and C-terminal NLS residues are underlined.

(B) Results of interaction assays in yeast with IMPa-4 bait and the various VirD2 deletion mutant preys. VirD2 interacts with IMPa-4 via residues Arg-372 to Arg-417. The *LacZ* activity was measured by liquid ONPG assays. Error bars represent SE of three biological replicates.

(C) Schematic representation of the various VirE2 deletion mutants used. VirE2 protein or its truncated derivatives are shown as gray boxes. VirE2 contains two central bipartite NLSs (black boxes). The NLS motifs are underlined.

(D) Results of interaction assays in yeast with IMPa-4 bait and the various VirE2 deletion mutant preys. VirE2 interacts with IMPa-4 via its two central NLS domains and also via the last 158 amino acids in its C terminus. Full-length and various deletion constructions of VirD2 preys, VirE2 preys, or the nonspecific GTPase prey were tested for interaction in yeast with IMPa-4 as a bait. The *LacZ* activity was measured by liquid ONPG assays. The *x* axis indicates the various bait plasmids used. Error bars represent SE of three biological replicates.

SSB and Importin α Binding of VirE2 Are Not Mutually Exclusive

Based on the partial overlap observed between the SSB domain and the NLSs of VirE2, several groups have argued that, once bound to T-strands, the NLSs of VirE2 may be inaccessible to nuclear import receptors and hence may not have a direct role in the nuclear import of the T-complex (Citovsky et al., 1992; Ziemienowicz et al., 2001). To investigate this, we performed gel mobility shift and supershift assays. We found that VirE2-bound ssDNA migrates at lower mobility and in a VirE2 dose-dependent manner through polyacrylamide gels in comparison with free ssDNA. Approximately 30 ng of His-tagged VirE2 was required to saturate 5 ng of labeled ssDNA (see Supplemental Figure 3 online). Furthermore, T7-tagged IMPa-4 decreased the mobility of a preformed ssDNA-VirE2 complex in a dose-dependent manner (Figure 4A, compare lane 2 with lanes 3 to 8). T7-tagged IMPa-4 protein did not bind to free ssDNA at the highest concentration tested (Figure 4A, lane 9). These results indicate that ssDNA-bound VirE2 protein maintains a conformation necessary for binding importin α.

We performed an additional in vitro gel mobility supershift assay in which His-tagged VirE2 was first incubated with an excess of T7-tagged IMPa-4. Following complex formation, we added labeled ssDNA. Figure 4B shows that VirE2 in a preformed IMPa-4-VirE2 complex can bind ssDNA (cf. lanes 2 and 3). These results support the previous observation that importin α–bound VirE2 maintains a conformation necessary to bind ssDNA. The SSB and importin α binding activities of VirE2, therefore, are not mutually exclusive.

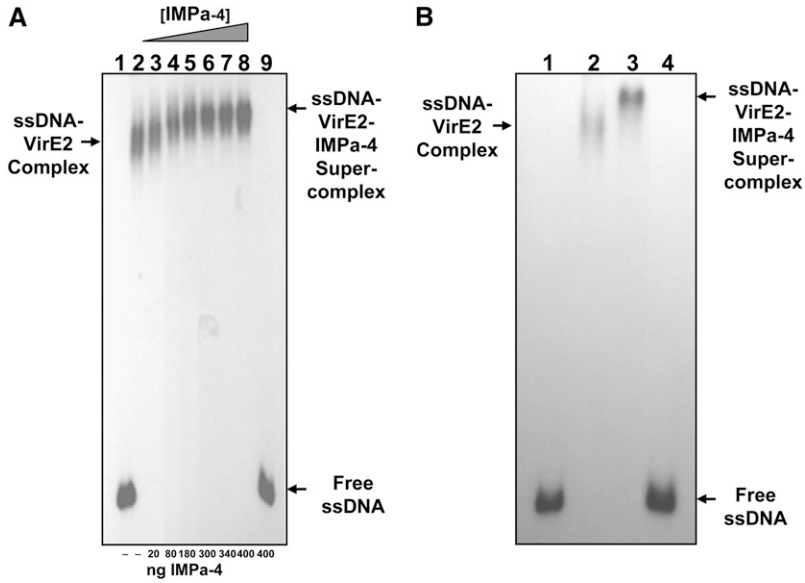

Figure 4. SSB and Importin α Binding Activities of VirE2 Are Not Mutually Exclusive.

(A) ssDNA-bound VirE2 protein binds importin α in vitro. ^{32}P end–labeled ssDNA complexed with 30 ng of His-VirE2 was incubated with increasing amounts (20 to 400 ng; amounts used are indicated below each lane) of T7–IMPa-4 protein. The samples were subjected to nondenaturing PAGE and visualized by autoradiography. Lane 1, labeled ssDNA; lanes 2 to 8, labeled ssDNA (5 ng) + VirE2 (30 ng) with increasing amounts of T7–IMPa-4 (20 to 400 ng); lane 9, labeled ssDNA (5 ng) + 400 ng of T7–IMPa-4.

(B) An importin α-VirE2 complex binds ssDNA in vitro. A total of 400 ng of IMPa-4 was preincubated with 30 ng of VirE2, and 5 ng of ^{32}P end–labeled labeled ssDNA was added before electrophoresis. Lane 1, labeled ssDNA; lane 2, labeled ssDNA (5 ng) + VirE2 (30 ng); lane 3, preincubated T7–IMPa-4 (400 ng) + VirE2 (30 ng) followed by 5 ng of labeled ssDNA; lane 4, labeled ssDNA (5 ng) + 400 ng T7–IMPa-4.

Several *Arabidopsis* Importin α Mutants Are Not Impaired in *Agrobacterium*-Mediated Transformation

Previous studies suggested that several importin α proteins may interact with VirD2 (Ballas and Citovsky, 1997; Bako et al., 2003). In order to determine the functional relevance of these interactions and whether specific importin α members are essential for *Agrobacterium*-mediated transformation, we investigated the transformation proficiency of *Arabidopsis* lines with T-DNA disruptions in some of the individual importin α genes. We identified plants homozygous for T-DNA insertions in *KAPα* (Salk_001092), *IMPa-2* (Salk_017914), and *IMPa-3* (Salk_025919). RT-PCR analysis indicated that full-length importin α transcripts were not detectable in the corresponding mutants (see Supplemental Figures 4A to 4C online). We tested the susceptibility of these mutant plants to transient (transfer of T-DNA not requiring integration) and stable *Agrobacterium*-mediated root transformation. T-DNA insertion lines individually harboring disruptions in each of these three genes were as susceptible to transformation by *Agrobacterium* as wild-type plants (Figure 5A). Figure 5B shows representative tumors observed on the roots of wild-type and importin α mutant plants. These data indicate that *KAPα*, *IMPa-2*, and *IMPa-3* are not individually essential for *Agrobacterium*-mediated root transformation.

An *Arabidopsis impa-4* Mutant Is a *rat* Mutant

Because the Salk collection did not contain an *impa-4* mutant, we screened the Feldmann T-DNA insertional mutant collection (ecotype Wassilewskija [Ws-2]) using a reverse genetics–based approach (Zhu et al., 2003). We identified a homozygous mutant containing a T-DNA disruption in the seventh intron of the *IMPa-4* gene (Figure 6A). RT-PCR analysis revealed only extremely low levels of *IMPa-4* transcript in this mutant (see Supplemental Figure 3D online). To quantify the amount of IMPa-4 protein synthesized in this mutant line, we generated a peptide antibody against amino acids 6 to 19. This region of the protein shares no significant homology with the other eight *Arabidopsis* importin α proteins, nor to other *Arabidopsis* proteins. Supplemental Figure 5 online shows that this peptide antibody reacts exclusively with IMPa-4. Using this specific antibody, we probed protein blots of extracts from leaf or root tissue from 4-week-old wild-type (ecotypes Columbia and Ws-2) and *impa-4* mutant plants. Figure 6B shows that IMPa-4 protein was detectable only in wild-type plants but not in *impa-4* plants. These results indicate that the T-DNA insertion in the seventh intron of *IMPa-4* does not permit the accumulation of importin α-4 protein.

Transient and stable transformation assays showed that *impa-4* is a *rat* mutant. *impa-4* mutant plants formed tumors at an efficiency sevenfold to eightfold lower than that of wild-type plants (Figure 6C). Whereas root segments from infected wild-type plants formed mostly large green teratomas, root segments from *impa-4* mutant plants formed mainly small yellow tumors. *impa-4* mutant plants have a greater than threefold reduction in transient transformation efficiency compared with wild-type plants (Figure 6C). Because transient expression requires nuclear import and conversion of the incoming ssT-DNA to a

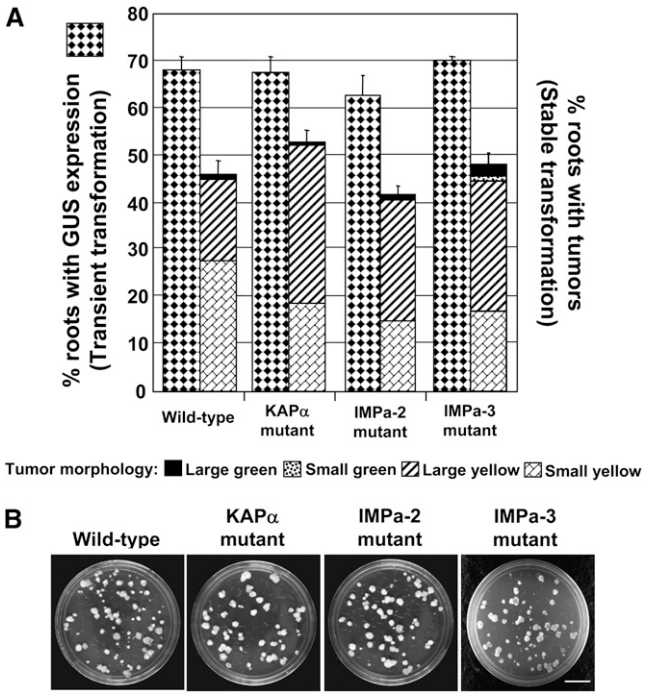

Figure 5. *Arabidopsis* Importin α Mutants *kapα*, *impa-2*, and *impa-3* Show Wild-Type *Agrobacterium*-Mediated Transformation Efficiencies.

(A) Root segments from *Arabidopsis* mutants homozygous for the disruption of *KAPα*, *IMPa-2*, or *IMPa-3* and wild-type control plants were infected with the tumorigenic strain *Agrobacterium* A208 (for stable transformation assays; multipatterned bars) or *Agrobacterium* strain At849 (containing a plant-active *gusA* gene for transient transformation assays; stippled black bars). Stable transformation efficiency (indicated by the presence of tumors) was scored and categorized after 1 month. The sizes and colors of the tumors are indicated by bar patterns. The larger and more green the tumors, the more highly susceptible the plant tissue is for transformation. For transient transformation, root segments were stained with 5-bromo-4-chloro-3-indolyl-β-glucuronic acid (X-gluc) at 6 d after infection, and the percentage of roots showing GUS activity was calculated. For each assay, 10 to 15 plants and >80 segments per plant were used. Error bars represent SE for the 10 to 15 plants assayed for each treatment.

(B) Representative plates showing tumorigenesis efficiencies (stable transformation) and tumor morphology on wild-type and importin α mutant root segments. Bar = 2 cm.

double-stranded transcription-competent form, the lower transient transformation efficiency of *impa-4* mutant plants indicates a hindrance in the transformation process at a step most likely prior to nuclear import of the T-complex. Thus, *IMPa-4* is important for an early step in *Agrobacterium*-mediated root transformation.

impa-4 RNA Interference Plants Show a rat Phenotype

To confirm that *IMPa-4* plays a role in *Agrobacterium*-mediated transformation, we generated *impa-4* RNA interference (RNAi) plants. The RNAi vector used to make these plants contained a hairpin construction of a region of the *IMPa-4* gene, mostly within the 3′ untranslated region (UTR), that does not show homology to other *Arabidopsis* importin α genes. We tested root segments from numerous T1 generation transgenic plants for transformation competence using the tumorigenic strain *Agrobacterium* A208. Figure 7 shows that silencing of *IMPa-4* by RNAi decreases susceptibility to *Agrobacterium*-mediated transformation for many of the RNAi lines. This result supports our previous findings that *IMPa-4* is involved in *Agrobacterium*-mediated transformation.

Arabidopsis Importin α Transcripts Are Differentially Expressed in Roots

In higher eukaryotes, importin α gene members demonstrate tissue-specific expression patterns and levels. This specificity likely reflects dynamic and regulated nucleocytoplasmic transport demands of individual tissues (Köhler et al., 1997). We performed real-time RT-PCR using primers specific to various importin α isoforms to investigate their expression levels in *Arabidopsis*. In roots, the investigated importin α isoforms display modest but significant differences in expression levels (Figure 8). *IMPa-4* transcripts accumulate in roots to levels 1.5- to 2-fold lower than those of *KAPα* and *IMPa-2*, respectively. Similarly, *IMPa-3* transcripts accumulate to levels threefold to fourfold lower than those of *KAPα* and *IMPa-2*, respectively. We also quantified the transcript levels of various importin α isoforms in flowers and leaves (see Supplemental Figure 6 online). The relative levels of expression in these tissues paralleled those seen in roots.

We performed a quantitative RT-PCR analysis to investigate whether the loss of *IMPa-4* transcripts in the *impa-4* mutant affects transcript levels of the other importin α isoforms. Figure 8 shows that in this mutant, levels of *IMPa-4* transcripts are greatly reduced (~250-fold) compared with those in wild-type plants. While the transcript levels of *KAPα* and *IMPa-2* were comparable in the *impa-4* mutant and wild-type roots, we detected a slight increase in *IMPa-3* transcript levels in the *impa-4* mutant relative to the wild type. Thus, the reduction of *IMPa-4* transcripts in the *impa-4* mutant is not compensated for by an increase in accumulation of the other importin α transcripts investigated.

Overexpression of Heterologous Importin α Isoforms Rescues the rat Phenotype of *impa-4* Mutant Plants

Although multiple isoforms of importin α interact with VirD2 and VirE2 in yeast and in vitro, only the *impa-4* mutant is a *rat* mutant. Thus, the other importin α isoforms are not redundant with IMPa-4 with respect to *Agrobacterium*-mediated transformation. This lack of redundancy could derive from several causes. The various importin α proteins could have different properties in planta (i.e., they may have different cargo preferences for transporting the T-complex to the nucleus). Alternatively, the various importin α proteins may be expressed at different levels, or with different patterns, in root cells. To address the apparent discrepancy between the interaction and the transformation assays, we hypothesized that if the level or expression pattern of *IMPa-4* was important for transformation, then constitutive overexpression of not only IMPa-4 but also of heterologous importin

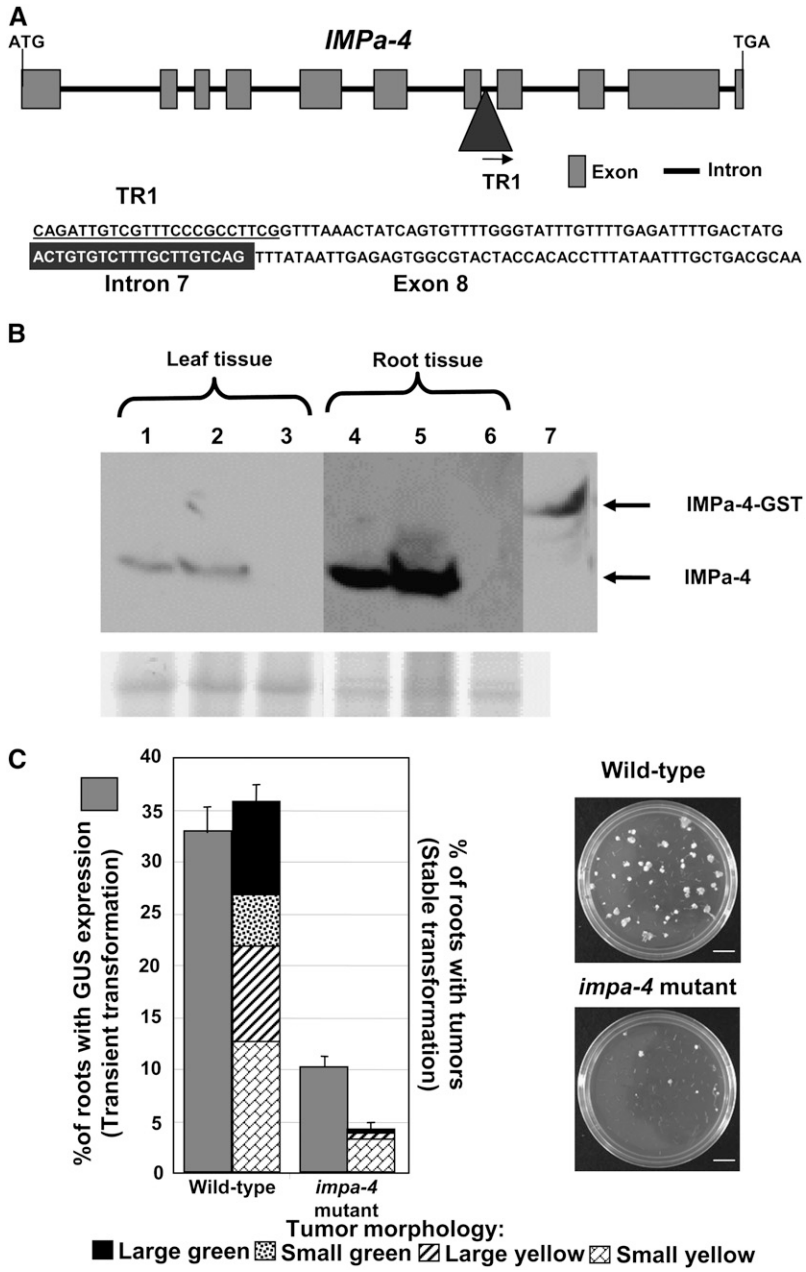

Figure 6. An *Arabidopsis impa-4* Mutant Is a *rat* Mutant.

(A) Schematic representation of the *IMPa-4* gene. The *Arabidopsis impa-4* mutant contains a T-DNA insertion in the seventh intron. A part of the T-DNA/plant DNA junction sequence is shown. The sequence corresponding to the T-DNA right border primer TR1 is underlined. The sequence for intron 7 (shaded box) is followed by a portion of exon 8 sequence. The position of the T-DNA right border TR1 primer is indicated with an arrow.

(B) Protein blot analysis of extracts isolated from leaf and root tissue of *Arabidopsis* ecotypes Ws-2 (lanes 1 and 4), Columbia (lanes 2 and 5), and *impa-4* mutant plants (lanes 3 and 6) with an antibody raised against an IMPa-4 peptide. Recombinant GST-tagged IMPa-4 protein was used as a control (lane 7). Top, immunostain; bottom, portion of a Coomassie blue–stained gel showing equal protein loading within each tissue sample.

(C) The *Arabidopsis impa-4* mutant shows reduced levels of transient and stable *Agrobacterium*-mediated root transformation. Root segments from wild-type and *impa-4* mutant plants were infected either with the tumorigenic strain *Agrobacterium* A208 (for stable transformation assays; multipatterned bars) or *Agrobacterium* At849 (for transient transformation assays; gray bars). For stable transformation, the tumors were scored after 1 month. For transient transformation, root segments were stained with X-gluc at 6 d after infection, and the percentage of roots showing GUS activity as a result of infection by *Agrobacterium* At849 was calculated. For each assay, 10 to 15 plants and >80 segments per plant were used. Error bars represent SE. Representative plates of tumorigenesis assays are shown. White bars = 1 cm.

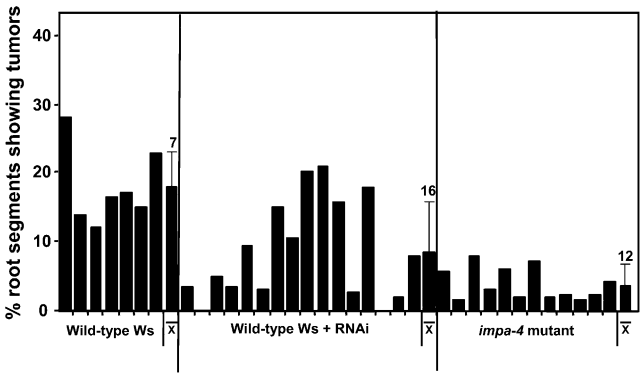

Figure 7. Inhibition of *Agrobacterium*-Mediated Root Transformation by Expression of an RNAi Construct Targeted Specifically against *IMPa-4*.

Root segments from wild-type (ecotype Ws-2), *impa-4* mutant, and RNAi plants were inoculated with *Agrobacterium* A208 at 10^7 colony-forming units/mL, and tumorigenesis assays were conducted. Tumors were scored after 6 weeks. Each bar indicates data from an individual plant, and average values for each set are indicated. Numbers above the error bars indicate the number of plants analyzed. Error bars indicate SE.

α isoforms should restore transformation competence to *impa-4* mutant plants. If, however, IMPa-4 plays a unique role in *Agrobacterium*-mediated transformation, then overexpression of only *IMPa-4* but not of other importin α isoforms would phenotypically complement the *impa-4* mutant.

Therefore, we generated individual transgenic lines in the *impa-4* mutant background overexpressing either an *IMPa-4* cDNA or cDNAs of other importin α isoforms. Transient and stable *Agrobacterium*-mediated transformation assays on independent lines of plants indicated that overexpression of not only *IMPa-4* but also of *KAPα*, *IMPa-2*, *IMPa-3*, *IMPa-6*, *IMPa-7*, and *IMPa-9* reversed the rat phenotype of the *impa-4* mutant (Figure 9; see Supplemental Tables 1A and 1B online). These results indicate that the rat phenotype of the *impa-4* mutant can be rescued by overexpression of other importin α isoforms, although *IMPa-6*, *-7*, and *-9* do so less efficiently than do *IMPa-1*, *-2*, *-3*, and *-4*.

Taken together, these data indicate that when the native expression levels of the tested importin α isoforms are overridden, they are functionally redundant with IMPa-4 with respect to *Agrobacterium*-mediated transformation.

Localization of VirD2 and VirE2 in Wild-Type and *impa-4* Mutant Plants

Previous studies have shown that when transiently expressed, both VirD2 and VirE2 proteins localize to the nuclei of plant cells (Howard et al., 1992; Tinland et al., 1992; Rossi et al., 1993; Citovsky et al., 1994; Guralnick et al., 1996; Mysore et al., 1998). In order to explore the cause of the rat phenotype of the *impa-4* mutant, we investigated the localization VirD2 and VirE2 in roots of *impa-4* mutant and wild-type plants. We generated transgenic wild-type and *impa-4* mutant plants overexpressing yellow fluorescent protein (YFP), YFP-VirE2, or VirE2-YFP fusion proteins. We were unable to generate transgenic plants expressing YFP fusions with full-length VirD2. Previous work in our laboratory indicated that transgenic plants overexpressing full-length VirD2 are nonviable (Hwang et al., 2006). Therefore, we generated transgenic plants expressing YFP fusions to the C-terminal *Nru*I (Arg-372 to Arg-417) fragment of VirD2 shown above as the domain necessary and sufficient for interaction with IMPa-4. We denote this fusion as YFP-VirD2*. T1 generation plants from several independent lines were analyzed for protein localization by confocal microscopy.

As expected, YFP alone localized throughout the cells of both wild-type and *impa-4* mutant roots (Figures 10A to 10D). In roots of both wild-type and *impa-4* mutant plants, YFP-VirD2* localized exclusively to the nucleus, as verified by the coincidence of YFP fluorescence and nuclear staining with Hoechst 33242 (Figures 10E to 10H). These results indicate that the *Nru*I (Arg-372 to Arg-417) fragment of VirD2 transfers foreign protein (in this case, YFP) to the nucleus. In addition, the data indicate that nuclear import of VirD2 is not compromised in roots of *impa-4* mutant plants.

YFP fluorescence in roots of transgenic plants expressing either YFP-VirE2 or VirE2-YFP never localized to the nucleus. In plants expressing YFP-VirE2, the fusion protein localized preferentially to the cell poles (Figures 10I and 10J, arrowheads). Tobacco BY-2 cells transiently expressing YFP-VirE2 also showed exclusive cytoplasmic localization of YFP fluorescence; this fluorescence was frequently in strands (see Supplemental Figure 7 online). Transgenic *Arabidopsis* roots expressing VirE2-YFP showed somewhat punctate aggregation in the cytoplasm (Figures 10M and 10N, arrowheads). Localization of YFP-VirE2 or VirE2-YFP fusion protein in roots of *impa-4* mutant plants was similar to that observed in roots of wild-type plants (Figures 10K, 10L, 10O, and 10P). These results indicate that the localization of VirE2, although nonnuclear, is unaffected by mutation of *impa-4*.

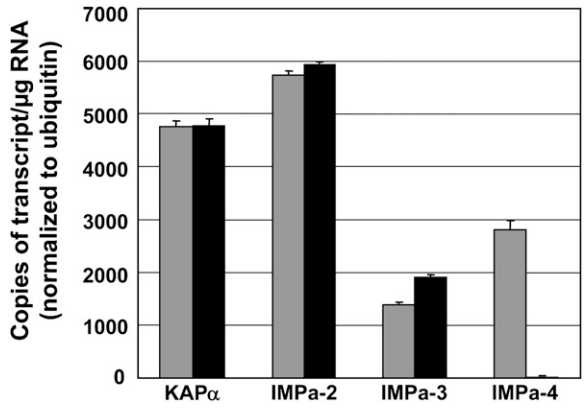

Figure 8. Differences in Transcript Levels of Various Importin α Isoforms in Wild-Type and *impa-4* Mutant Roots as Determined by RT-PCR.

Total RNA from wild-type and *impa-4* mutant roots was reverse-transcribed using oligo(dT) primers and then subjected to real-time PCR analysis using various importin α gene-specific primers. RT-PCR with ubiquitin primers was performed as a control to correct for sample concentrations. Gray and black bars represent the transcript levels of the indicated importin α isoforms in wild-type and *impa-4* mutant roots, respectively. Error bars represent SE of four technical replicates.

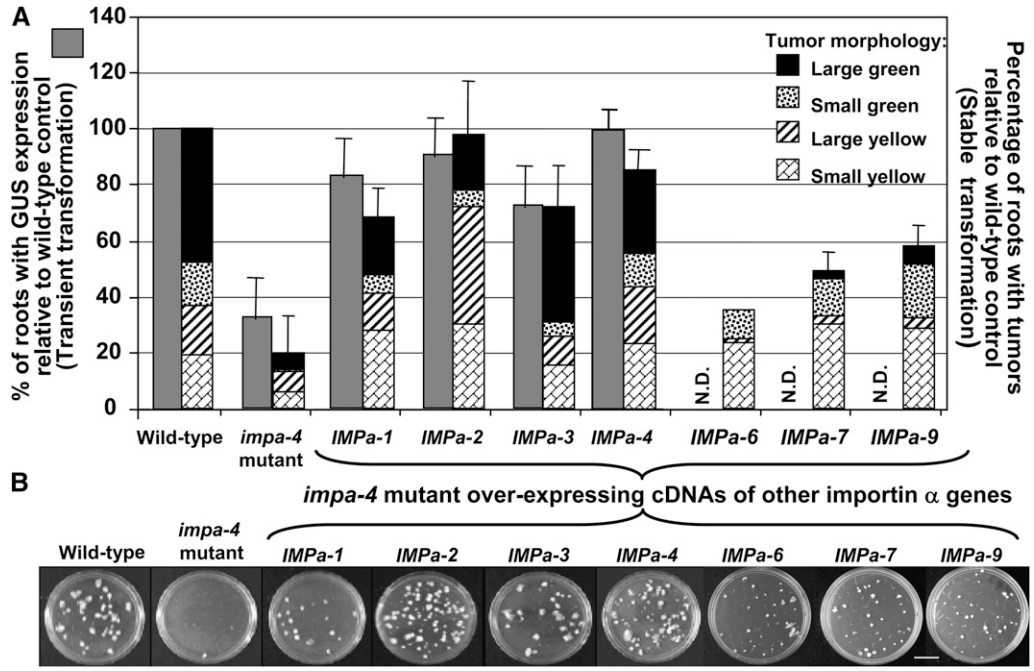

Figure 9. Overexpression of Importin α Isoforms Rescues the Rat Phenotype of *impa-4* Mutant Roots.

(A) Transgenic plants individually overexpressing At *KAPα*, *IMPa-2*, *IMPa-3*, *IMPa-4*, *IMPa-6*, *IMPa-7*, or *IMPa-9* cDNAs in the *impa-4* mutant background show increased susceptibility to *Agrobacterium*-mediated root transformation compared with parent *impa-4* mutant plants. Root segments from several T2 generation transgenic plants (2 to 3 independent lines each for *KAPα*, *IMPa-2*, *IMPa-3*, or *IMPa-4* overexpression) or T1 generation transgenic plants (14 to 15 independent plants each for *IMPa-6*, *IMPa-7*, or *IMPa-9* overexpression) were infected with either the tumorigenic strain *Agrobacterium* A208 (for stable transformation assays; multipatterned bars) or *Agrobacterium* At849 (for transient transformation assays; gray bars). Infected root segments from wild-type and *impa-4* mutant plants were used as positive and negative controls, respectively. For stable transformation, the tumors were scored after approximately 1 month. For transient transformation, root segments were stained with X-gluc at 6 d after infection, and the percentage of roots showing GUS activity resulting from infection by *Agrobacterium* At849 was calculated. N.D., not determined. Error bars indicate SE.

(B) Representative plates of tumorigenesis assays. Bar = 2 cm.

VirE2 can form multimers utilizing specific peptide domains (Citovsky et al., 1997; Dombek and Ream, 1997; Zhou and Christie, 1999). We used BiFC (Citovsky et al., 2006) to investigate the subcellular site of VirE2–VirE2 interaction in electroporated tobacco BY-2 cells. In BiFC, a YFP molecule is split into two sections, neither of which fluoresces on its own. Refolding of the two partial YFP moieties restores fluorescence (fluorescence complementation). Refolding can occur if each YFP moiety is affixed to proteins that themselves interact, thus bringing together the YFP peptides (Hu et al., 2002). Figure 11A and Supplemental Table 2 online show that VirE2 proteins interact with each other; interaction localizes exclusively to the cytoplasm, confirming the cytoplasmic localization of VirE2 shown in Figures 10 and 11.

Our observation that the VirE2 fusion protein localized to the cytoplasm differs from the findings of others, in which a β-glucuronidase (GUS) protein fused to the N terminus of VirE2 localized to the nucleus (Citovsky et al., 1992, 1994; Guralnick et al., 1996; Li et al., 2005). Because it is possible that protein tags may alter protein function, we tested the functionality of our VirE2 fusion proteins using root-based extracellular complementation (Otten et al., 1984) transient transformation assays on transgenic *Arabidopsis* plants expressing either YFP-VirE2 or VirE2-YFP. We inoculated root segments of these plants with *Agrobacterium* At1565, a *virE2*$^-$ mutant strain containing the T-DNA binary vector pBISN1 (Narasimhulu et al., 1996). As a positive control for extracellular complementation, we used a transgenic *Arabidopsis* line expressing untagged VirE2. The results of these assays showed that roots of transgenic plants expressing VirE2-YFP, but not YFP-VirE2, were transformable by At1565 (Figure 12). The transient transformation efficiency was comparable to that of the positive control plants. As expected, roots of wild-type *Arabidopsis* plants were not transformed by the *virE2*$^-$ mutant *Agrobacterium* strain. These results indicate that, with respect to *Agrobacterium*-mediated transformation, a VirE2-YFP fusion protein retains functionality whereas a fusion to the N terminus of VirE2 (YFP-VirE2) does not.

Several Importin α Isoforms Can Interact with VirD2 and VirE2 in Planta

We used BiFC to examine whether interactions between virulence proteins D2 or E2 and various importin α proteins could also occur in plants. Supplemental Table 2 online and Figures

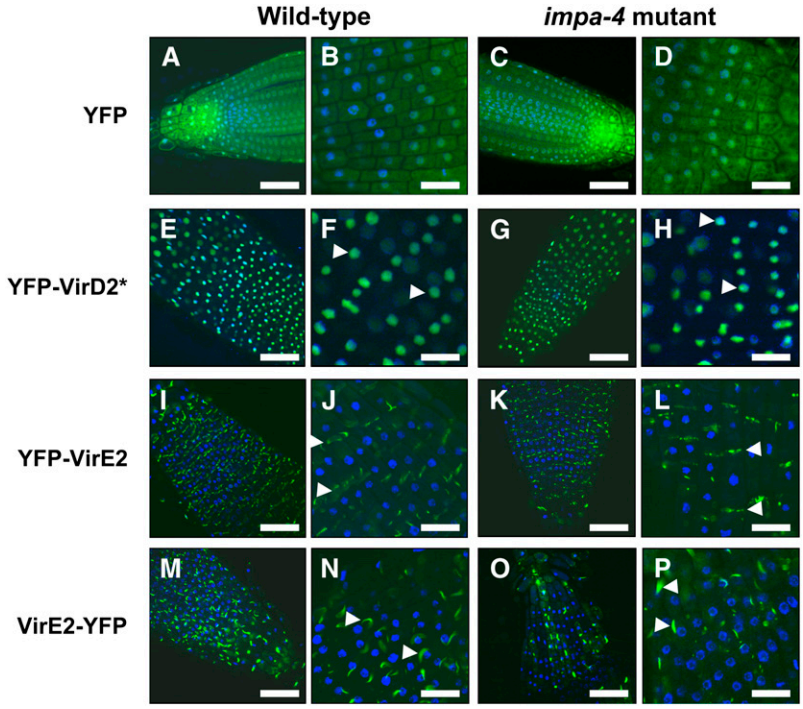

Figure 10. Localization of YFP-VirD2, YFP-VirE2, and VirE2-YFP in Wild-Type and *impa-4* Mutant Roots.

Single-plane confocal optical sections show YFP localization (green fluorescence) throughout cells (both in the cytoplasm and in the nucleus) in the root tip of wild-type (**[A]** and **[B]**) and *impa-4* mutant (**[C]** and **[D]**) plants. YFP-VirD2 preferentially localizes to the nuclei of root tip cells of both wild-type (**[E]** and **[F]**) and *impa-4* mutant (**[G]** and **[H]**) plants. YFP-VirD2 colocalizes with nuclear Hoechst 33242 stain (blue fluorescence). In both wild-type (**[I]** and **[J]**) and *impa-4* mutant (**[K]** and **[L]**) root tip cells, YFP-VirE2 localizes at cell poles (arrowheads). VirE2-YFP also aggregates in the cytoplasm (arrowheads) in both wild-type (**[M]** and **[N]**) and *impa-4* mutant (**[O]** and **[P]**) root tip cells. In **(A)** to **(L)**, blue indicates Hoechst 33242 staining of nuclei. Bars = 15 μm in **(A)**, **(C)**, **(E)**, **(G)**, **(I)**, **(K)**, **(M)**, and **(O)** and 50 μm in **(B)**, **(D)**, **(F)**, **(H)**, **(J)**, **(L)**, **(N)**, and **(P)**.

11B to 11E show that nYFP-VirD2 interacted with KAPα–cYFP, IMPa-4–cYFP, IMPa-7–cYFP, and IMPa-9–cYFP. In these experiments, the proteins were expressed from cDNA clones under the regulation of a cauliflower mosaic virus (CaMV) 35S promoter. The interacting protein partners localized to the nucleus, confirming the localization results shown in Figures 10E and 10F. By contrast, VirE2-nYFP interacted with these importin α proteins mostly in the cytoplasm (Figures 12G to 12K; see Supplemental Table 3 online), confirming the results shown in Figures 10M and 10N. However, YFP fluorescence sometimes localized to the nucleus, especially with IMPa-4 (Figure 11I). These results suggest that IMPa-4 may be more efficient at delivering VirE2 to the nucleus than KAPα is, again indicating the importance of IMPa-4 in *Agrobacterium*-mediated transformation.

It is possible that overexpression of *IMPa-4* from the CaMV 35S promoter may result in mislocalization of the interacting protein partners. Therefore, we constructed a plasmid that would express IMPa-4–cYFP at native levels. This construction contained the *IMPa-4* promoter, introns, exons, and 3′ UTR. Figures 11F and 11L show that when expressed from this plasmid, IMPa-4 again interacted with VirD2 in the nucleus and with VirE2 predominantly in the cytoplasm.

In the BiFC experiments described above, we could visualize the interaction of VirD2 or VirE2 with only one importin α isoform at a time. It is possible, however, that these Vir proteins interact simultaneously with several importin α isoforms. Therefore, we conducted multicolor BiFC experiments, as described by Hu and Kerppola (2003). In these experiments, the Vir protein (either VirD2 or VirE2) was tagged with cCFP (for cyan fluorescent protein), and the importin α partners were tagged with either nVenus or nCerulean (Shyu et al., 2006). Expression cassettes encoding the tagged Vir protein and both of the tagged importin α proteins were transiently transfected into tobacco BY-2 cells. Interaction of the Vir protein with importin α tagged with nVenus would generate yellow/green fluorescence, whereas interaction of the Vir protein with importin α tagged with nCerulean would generate blue fluorescence. To indicate whether cells were competent to receive DNA, we cotransfected the cells with an expression cassette that expressed mCherry; these cells would fluoresce red. As a control, we swapped nGFP (for green fluorescent protein) derivative fluorescent tags on the importin α proteins.

Figures 13A to 13H show that VirD2 could simultaneously interact with both IMPa-1 and IMPa-4. In each instance, interaction occurred in the nucleus, validating the results shown in Figures 11B and 11C. The interaction of VirE2 with IMPa-1 and IMPa-4 was more complex. Interaction of VirE2 with IMPa-1 always occurred in the cytoplasm (Figures 13J and 13N),

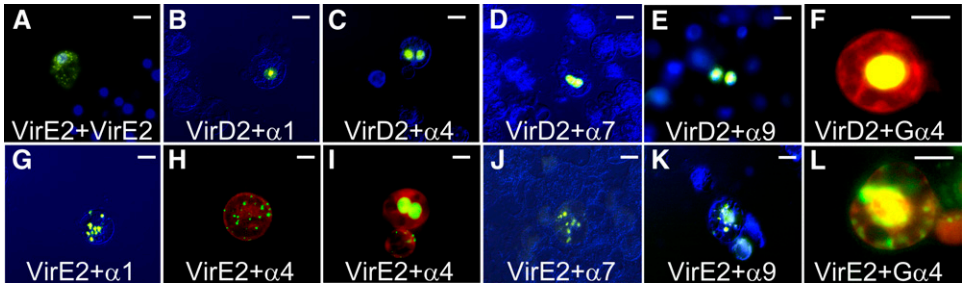

Figure 11. Interaction and Localization of VirE2 with Itself and of VirD2 and VirE2 with Importin α Proteins in Plant Cells.

BiFC constructs were electroporated into tobacco BY-2 cells, and the cells were visualized by fluorescence microscopy 48 h later. Constructs are as follows: VirE2-nYFP plus VirE2-cYFP **(A)**; nYFP-VirD2 plus KAPα-cYFP **(B)**; nYFP-VirD2 plus IMPa-4–cYFP **(C)**; nYFP-VirD2 plus IMPa-7–cYFP **(D)**; nYFP-VirD2 plus IMPa-9–cYFP **(E)**; nYFP-VirD2 plus IMPa-4–cYFP genomic clone **(F)**; VirE2-nYFP plus KAPα-cYFP **(G)**; VirE2-nYFP plus IMPa-4–cYFP (**[H]** and **[I]**); VirE2-nYFP plus IMPa-7–cYFP **(J)**; VirE2-nYFP plus IMPa-9–cYFP **(K)**; VirE2-nYFP plus IMPa-4–cYFP genomic clone **(L)**. In **(A)** and **(E)**, blue indicates Hoechst 33242 staining of nuclei. In **(B)**, **(C)**, **(D)**, **(G)**, **(J)**, and **(K)**, blue indicates false-color image of the entire cell. In **(F)**, **(H)**, **(I)**, and **(L)**, red fluoresecent protein images (marking the entire cell) are merged with the YFP images. Bars = 20 μm.

confirming the results shown in Figure 11G. However, interaction of VirE2 with IMPa-4 occurred both in the nucleus and in the cytoplasm (Figures 13K and 13O), confirming the results shown in Figures 11H and 11I. Swapping the fluorescent tags on the two importin α proteins did not alter these results. Thus, VirE2 localized to the nucleus only when IMPa-4, but not IMPa-1, was overexpressed. These results again suggest the importance of IMPa-4 in the transformation process.

DISCUSSION

Several Importin α Isoforms Interact with both VirD2 and VirE2

Importin α proteins in *Arabidopsis* are encoded by a multigene family consisting of nine members (Figure 1; see Supplemental Figure 1 online). In this study, VirD2 and VirE2 interacted in yeast and in vitro with each of four importin α isoforms tested (KAPα and IMPa-2, -3, and -4; Figure 2). VirD2 and VirE2 additionally interacted in plants with IMPa-7 and IMPa-9 (Figure 11). The interaction of VirD2 with KAPα, IMPa-3, and IMPa-4 in yeast is consistent with the reports of Ballas and Citovsky (1997) and Bako et al. (2003). Our finding that VirE2 also interacts with these importin α isoforms contrasts with the observations of Ballas and Citovsky (1997), who failed to detect an interaction between VirE2 and KAPα. Ballas and Citovsky (1997) expressed VirE2 as a bait protein and KAPα as a prey protein, whereas we expressed VirE2 as a prey and the various importin α isoforms as baits. It is possible that when VirE2 is used as a prey but not as a bait the fusion may maintain a conformation necessary to interact with importin α proteins. Interaction of VirD2 and VirE2 with IMPa-4 in plants cannot be attributed to overexpression of the importin α protein, because expression of tagged IMPa-4 at normal levels from its native gene context also indicated interaction with these virulence proteins (Figure 11F).

To identify domains of VirD2 and VirE2 that are important for interaction with importin α, we tested the interaction of a series of VirD2 and VirE2 deletion mutants with IMPa-4 as the prototype importin α member (Figure 3). We chose this isoform for these experiments because mutational analysis of the various importin α genes indicated that in *Arabidopsis*, IMPa-4 is the only isoform tested that is required for *Agrobacterium*-mediated root transformation (Figures 5 and 6). The *Agrobacterium* VirD2 protein contains N-terminal and C-terminal regions of amino acids resembling those found in classical monopartite and bipartite NLSs, respectively (Robbins et al., 1991). Based on various mutations, the N-terminal NLS was proposed not to be essential for the nuclear import of T-strands (Shurvinton et al., 1992; Rossi et al., 1993). This NLS does not interact with IMPa-4 (Figure 3B). Sequences resembling classical NLSs are not always recognized by importin α (Neumann et al., 1997; Wang et al., 1997).

The VirD2 C-terminal bipartite NLS, which has been suggested to play a role in the nuclear import of T-strands (Rossi et al., 1993), was not essential for interaction with importin α. Truncated VirD2 with a precise deletion of the C-terminal NLS residues (deletions of KRPR and KRAR) still interacted in yeast with IMPa-4, although at a slightly lower level than did wild-type VirD2 (Figures 3A and 3B). This observation is in contrast with that of Ballas and Citovsky (1997), who reported a complete abolition of KAPα interaction with a VirD2 protein containing a precise deletion of the C-terminal bipartite NLS residues (deletions of KRPR and RKRER). Although the reason for these differences is not clear, the use of slightly different deletion mutants may have resulted in these contradictory observations. Our assays showed that an internal deletion of 45 amino acid residues (Arg-372 to Arg-417) that include the bipartite NLS (VirD2Δ*Nru*I) abolished interaction of the mutant VirD2 protein with IMPa-4. This result suggests that, whereas the C-terminal NLS of VirD2 may modulate the strength of interaction with importin α, additional adjoining residues are also important for this interaction. Our interaction results are consistent with previous reports showing that virulence of a mutant *Agrobacterium* strain with precisely the same deletion of the VirD2 C-terminal NLS residues (VirD2ΔNLS) shows little reduction in transformation (Shurvinton et al., 1992; Mysore et al., 1998). By contrast, a strain expressing the same VirD2Δ*Nru*I protein that we examined in this report was avirulent (Shurvinton et al., 1992) or severely compromised in virulence (Rossi et al., 1993). Taken together,

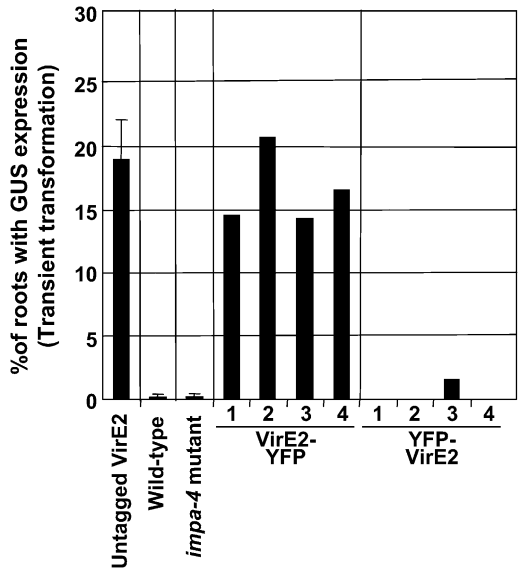

Figure 12. Wild-Type and *impa-4* Mutant Roots Overexpressing VirE2-YFP, but Not YFP-VirE2, Complement a *virE2* Mutant *Agrobacterium* in Transient Transformation Assays.

Several independent T1 transgenic plants overexpressing YFP-VirE2 or VirE2-YFP in the wild type or in the *impa-4* mutant background were infected with *Agrobacterium* At1565. Root segments were stained with X-gluc at 6 d after infection, and the percentage of roots showing GUS activity resulting from infection by *Agrobacterium* At89 was calculated. Root segments from wild-type plants overexpressing untagged VirE2 were used as positive controls (left bar). Nontransgenic wild-type plants and *impa-4* mutant plants were used as negative controls. For each assay, >80 segments per plant were used. Error bars represent SE.

our results suggest that a 46–amino acid region (Arg-372 to Arg-417) of octopine-type VirD2 that includes the C-terminal NLS and adjoining amino acids is important for nuclear import of T-strands, presumably through interactions with importin α.

Interaction assays of various VirE2 deletion mutants with IMPa-4 in yeast further support the specificity of the VirE2 interaction with importin α (Figure 3). Interaction of VirE2 proteins containing both bipartite NLSs results in a higher level of β-galactosidase activity than does VirE2 containing only one NLS. This observation is in agreement with that of Citovsky et al. (1992), who reported that efficient nuclear import of VirE2 requires both NLSs.

Importin α May Mediate T-Strand Nuclear Import via Interactions with VirE2

The T-complex is proposed to consist of multiple molecules of VirE2 coating the T-strand, which is covalently linked at its 5′ terminus to VirD2. VirE2 presumably protects T-strands from nucleolytic attack in the plant (Yusibov et al., 1994; Rossi et al., 1996). The partial overlap of the ssDNA binding domain and the second NLS of VirE2 raises the question of whether VirE2 NLSs are accessible to plant nuclear import components once VirE2 protein is bound to the T-strand. Our in vitro gel mobility supershift results (Figure 4) suggest that the ssDNA and importin α binding activities of VirE2 are not mutually exclusive and that VirE2 can mediate the nuclear import of T-strands in an importin α–dependent manner.

Tzfira et al. (2001) identified VIP1, an *Arabidopsis* basic Leu zipper protein, which interacts with VirE2. VIP1 also interacts with KAPα (Tzfira et al., 2002). Because they were unable to demonstrate interaction of VirE2 with KAPα, these authors suggested that VIP1 may serve as an adaptor molecule to facilitate the import of VirE2-bound T-strands into the nucleus. Our data demonstrate, however, that VirE2 can directly bind all tested importin α isoforms (KAPα and IMPa-2, -3, -4, -7, and -9; Figures 2 and 11). It is possible that VirE2 may utilize several cellular mechanisms for nuclear import, thereby creating additional opportunities for T-complex entry into the nucleus.

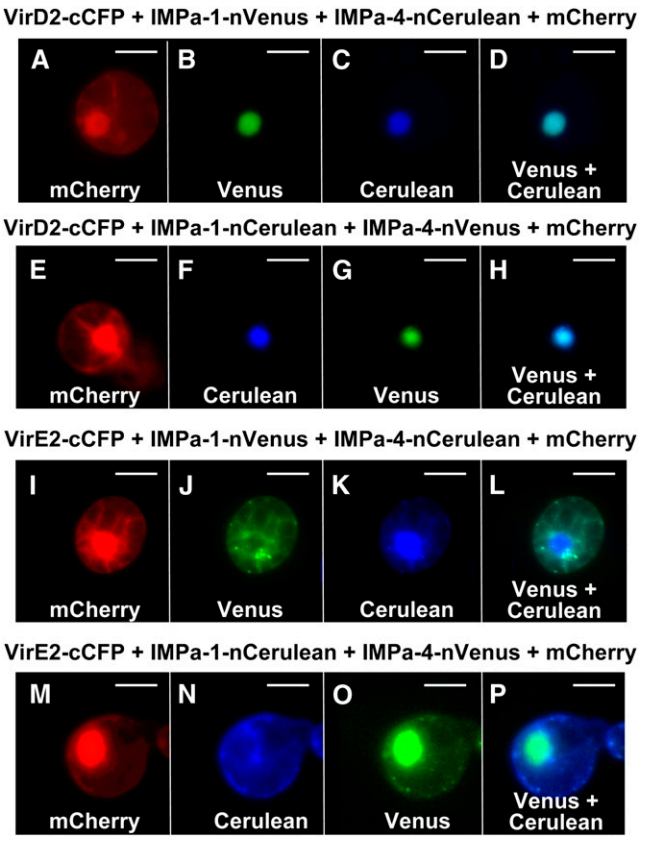

Figure 13. Multicolor BiFC Indicates the Site of Interaction of VirD2 and VirE2 with IMPa-1 (KAPα) and IMPa-4.

VirD2-cCFP (**[A]** to **[H]**) and VirE2-cCFP (**[I]** to **[P]**) were used as baits to interact simultaneously with IMPa-1 or IMPa-4. mCherry indicates transfected BY-2 protoplasts; red fluorescence localizes both to the cytoplasm and to the nucleus. The various combinations of labeled proteins coexpressed in the protoplasts are indicated above each series of four panels. Cells were visualized using an epifluorescence microscope: **(A)**, **(E)**, **(I)**, and **(M)**, red (mCherry) channel; **(B)**, **(G)**, **(J)**, and **(O)**, yellow/green (Venus) channel; **(C)**, **(F)**, **(K)**, and **(N)**, blue (Cerulean) channel; **(D)**, **(H)**, **(L)**, and **(P)**, overlay of yellow and blue channels. Bars = 20 μm.

With Regard to T-Complex Nuclear Import, to What Extent Are Importin α Isoforms Redundant?

The interaction of VirD2 and VirE2 with several *Arabidopsis* importin α isoforms suggests redundancy. However, disruption of only *IMPa-4*, but not *KAPα*, *IMPa-2*, or *IMPa-3*, reduced *Agrobacterium*-mediated root transformation of *Arabidopsis*. Relative to wild-type plants, the *impa-4* mutant expresses greatly reduced amounts of *IMPa-4* mRNA and undetectable levels of IMPa-4 protein (Figures 6 and 8). Disruption of *IMPa-4* expression was not compensated for by increased expression of the other importin α genes examined (Figure 8). Therefore, we investigated whether manipulation of native expression patterns and levels of heterologous importin α genes, by overexpression from a constitutive CaMV 35S promoter, could phenotypically complement the transformation deficiency of the *impa-4* mutant. Overexpression not only of *IMPa-4* but also of *KAPα*, *IMPa-2*, *IMPa-3*, *IMPa-6*, *IMPa-7*, and *IMPa-9* restored transformation competence to the *impa-4* mutant, showing functional redundancy among these importin α proteins (Figure 9). The rat phenotype of the *impa-4* mutant, in which the other importin α genes are expressed, likely results from differing patterns of importin α gene expression, especially in those root cells most susceptible to transformation (Yi et al., 2002, 2006). Our observations are similar to those of Mason et al. (2002), who reported complementation of male sterility defects in *Drosophila* resulting from loss of importin α-2 by overexpression of either α-2 or of the heterologous α-1 and α-3 transgenes.

Subcellular Localization of VirD2 and VirE2 in Wild-Type and *impa-4* Mutant Plants

The lack of transformation proficiency of the *impa-4* mutant could result from the inability of this plant to support nuclear localization of VirD2 and/or VirE2 and, thus, the T-complex. To test this, we examined the localization of YFP-VirD2*, YFP-VirE2, and VirE2-YFP fusions in wild-type and *impa-4* mutant plants. YFP-VirD2* localized to the nucleus in both wild-type and *impa-4* mutant plants, suggesting that the rat phenotype of these plants did not result from lack of VirD2 nuclear import (Figures 10A to 10H).

We did not detect nuclear localization of either YFP-VirE2 or VirE2-YFP fusion protein in roots of wild-type or *impa-4* plants (Figures 10I to 10P). Whereas YFP-VirE2 localized to the cell poles, VirE2-YFP showed cytoplasmic aggregation that sometimes resulted in punctate patterns. These results contrast with previous reports indicating that transiently expressed VirE2 (with either a fluorescent tag or as a fusion with reporter GUS or GFP proteins) localized to nuclei (Citovsky et al., 1992, 1994; Zupan et al., 1996; Tzfira et al., 2001; Ziemienowicz et al., 2001). Our results, however, are consistent with the observation that VirE2 can associate with membranes (Dumas et al., 2001; Duckely et al., 2005) and remains in the cytoplasm (Duckely and Hohn, 2003). Indeed, Grange et al. (2008) recently showed that when tobacco BY-2 cells were bombarded with a VirE2-hemagglutinin expression construct, VirE2 localized exclusively to the cytoplasm. Our results further demonstrate that VirE2 localization in *impa-4* mutant roots does not differ from that observed in wild-type plants.

Several reports delineating the functional domains of VirE2 suggested that some mutations or tag insertions in VirE2 may render the resulting protein either nonfunctional or may interfere with the ssDNA binding or cooperativity of VirE2 (Dombek and Ream, 1997; Simone et al., 2001). Therefore, we investigated whether the observed lack of nuclear localization of YFP-VirE2 or VirE2-YFP resulted from altered properties conferred by the YFP tag. To test for functionality of the two VirE2 fusions, we infected roots of transgenic plants expressing either YFP-VirE2 or VirE2-YFP with the *virE2*$^-$ mutant strain *Agrobacterium* At1565. Our assays showed that wild-type plants expressing VirE2-YFP, but not YFP-VirE2, were susceptible to transformation by *Agrobacterium* At1565 at levels comparable to those of transgenic plants expressing untagged VirE2 (Figure 12). These results demonstrate that VirE2-YFP, but not YFP-VirE2, is fully functional with respect to *Agrobacterium*-mediated transformation, despite its inability to localize to the nucleus.

T-strands affixed to VirD2 and VirE2 are transferred independently from *Agrobacterium* to the plant cell (Binns et al., 1995; Lee et al., 1999; Vergunst et al., 2000), where they are likely assembled into a mature T-complex. Our observation that VirE2 localizes predominantly to the cytoplasm (Figures 11 and 13; see Supplemental Figure 6 online) is consistent with this model. BiFC indicated that cytoplasmic VirE2 associates with importin α. However, when coexpressed with IMPa-4, some of the pool of VirE2 may move to the nucleus (Figures 11 and 13). These observations may explain the role of VirE2 in protecting T-strands against nucleolytic degradation in the plant cytoplasm (Yusibov et al., 1994) and its role in the nuclear import of the T-complex (Gelvin, 1998; Ziemienowicz et al., 2001). Whether some of the cytosolic VirE2 localizes to the nucleus after forming a complex with T-strands requires further investigation.

Our findings that mutation of *IMPa4* reduces *Agrobacterium*-mediated transformation but does not apparently affect the localization of T-complex components VirD2 and VirE2 may at first appear contradictory. We speculate that only a small portion of the cytoplasmic VirE2 population may participate in T-strand nuclear transport and that this subpopulation is below our level of detection using our imaging assays. Alternatively, VirD2 and VirE2 may behave differently when complexed with T-strands compared with our investigations that imaged free protein molecules. Finally, IMPa-4 may be responsible for nuclear targeting of other bacterial or plant proteins, which we have not investigated, that are important for transformation. Future investigations into the mechanism of T-complex assembly, cytoplasmic trafficking, and nuclear import will contribute not only to our knowledge of *Agrobacterium*-mediated transformation but also to a better understanding of the nuclear import of protein–nucleic acid complexes.

METHODS

Phylogenetic Analysis of the Nine *Arabidopsis* Importin α Proteins

Sequence searches of the *Arabidopsis thaliana* genome identified nine importin α isoforms. These are *KAPα*/*IMPa-1* (At3g06720), *IMPa-2* (At4g16143), *IMPa-3* (At4g02150), *IMPa-4* (At1g09270), *IMPa-5* (At5g49310), *IMPa-6* (At1g02690), *IMPa-7* (At3g05720), *IMPa-8*

(At5g52000), and *IMPa-9* (At5g03070). The proteins encoded by these genes were aligned using the ClustalW module of the MegAlign 7.1 program (DNASTAR). The sequence alignment is shown in Supplemental Figure 1 online and was used for the construction of a cladogram. In the phylogenetic tree, construction bootstrapping was performed for 1000 replicates with a seed of 111.

PCR Amplification of *Arabidopsis* Importin α cDNAs

Total RNA was extracted from 2- to 3-week-old plants using TRIZOL reagent (GIBCO) following the instructions provided by the manufacturer. Two micrograms of total RNA was reverse-transcribed using poly(dT) primers and AMV reverse transcriptase (Promega) to obtain single-stranded cDNA. Double-stranded cDNA synthesis was performed using the gene-specific primer sequences presented in Supplemental Table 3 online. Except for primers used to amplify *IMPa-6*, all forward primers contained a 5′-*Eco*RI restriction endonuclease site followed by sequences from the second codon. Reverse primers contained a 5′-*Bam*HI restriction endonuclease site followed by sequences including the stop codon. *IMPa-6* forward primers contained *Sal*I and *Bgl*II sites, and the reverse primer contained a *Sac*I site. PCR was performed in a 50-μL reaction volume with 2 units of Pwo polymerase (Roche). PCR amplification conditions were as follows: 95°C for 5 min (1 cycle); 95°C for 40 s, 58°C for 1 min, and 72°C for 5 min (36 cycles); and 72°C for 1 min (1 cycle). The PCR products were cloned into pBluescript KS+ (Stratagene) and verified by sequencing (Purdue Sequencing Facility).

Yeast Two-Hybrid Plasmid Construction and Assays

From the plasmids mentioned above, the corresponding importin α cDNAs were individually subcloned as *Eco*RI-*Bam*HI fragments into bait and prey vectors pSTT91 and pGAD424, respectively (Clontech). The constructed plasmids and the bait and prey clones expressing full-length and truncated forms of octopine VirD2 (Hwang et al., 2006) and VirE2 are shown in Supplemental Table 4 online. As negative controls, empty baits, empty preys, or an *Aspergillus nidulans* GTPase protein were used as prey plasmids (see Supplemental Table 4 online). Yeast transformations were performed using the lithium acetate method (Becker and Lundblad, 1994). The cells were plated onto synthetic dropout–agar plates lacking the appropriate amino acids and incubated for 2 d at 30°C. Interactions were tested qualitatively by transferring the yeast transformants to synthetic dropout–agar plates containing the chromogenic substrate 5-bromo-4-chloro-3-indolyl-β-D-galactopyranoside. The plates were incubated for 2 d at 30°C. Positive interactions were detected by the expression of the reporter *LacZ* gene that converts the substrate 5-bromo-4-chloro-3-indolyl-β-D-galactopyranoside to an insoluble blue dye, 5-bromo 4-choloro indole.

Quantitative β-galactosidase assays, using ONPG (Sigma-Aldrich) as substrate, were performed on three independent colonies of each bait–prey combination. The assay was performed according to the protocol in the Matchmaker two-hybrid system user manual (Clontech). The absorbance of the reaction fluids was measured using a spectrophotometer (Spectra Max Plus 384; Molecular Devices). Protein quantification of the cell suspensions was performed using a Bradford assay. β-Galactosidase activity was reported as micromoles of ONPG hydrolyzed per minute per milligram of total protein.

Recombinant Protein Expression, Purification, and in Vitro Protein Binding Assays

Plasmids expressing recombinant importin α proteins were tagged on their N termini by GST or T7 epitope and are listed in Supplemental Table 4 online. The expression vectors for various tagged and untagged versions of either the full-length or truncated forms of VirD2 and VirE2 proteins are also described in Supplemental Table 4 online.

The expression and purification of GST fusion proteins were performed according to Ausubel et al. (2003) with some minor modifications. Isopropyl β-D-thiogalactopyranoside–induced *Escherichia coli* BL21 (DE3) cells containing the corresponding expression plasmids were collected by centrifugation and resuspended in chilled PBS containing 1 mM DTT and 1 mM phenylmethylsulfonyl fluoride (PMSF). Cell lysis was performed with 0.5 mg/mL (w/v) chicken egg white lysozyme (Sigma-Aldrich) for 2 h on ice. Triton X-100 was added to the cell suspension to a final concentration of 1% (v/v) and gently mixed by inversion. The lysate was centrifuged at 12,000 rpm for 30 min at 4°C to remove cell debris. The supernatant solution was added to PBS-preswelled glutathione–Sepharose beads (Sigma-Aldrich) to enable the GST fusion proteins to bind overnight at 4°C. The next day, the slurry of beads and supernatant solution was transferred to a column and the supernatant solution was allowed to flow through the column. The column containing the glutathione–Sepharose beads was washed with 25 bed volumes of chilled PBS containing DTT and PMSF. These glutathione–Sepharose beads containing the bound GST fusion proteins either were used directly for the in vitro GST pull-down assay (described below) or the bound proteins were eluted from the beads. Bound proteins were eluted in 1-mL fractions with chilled 50 mM Tris-HCl (pH 8) containing 5 mM reduced glutathione (Sigma-Aldrich). The fractions were analyzed by SDS-PAGE, and proteins were visualized by staining with Coomassie Brilliant Blue R 250.

Purification of T7-tagged importin α proteins was performed according to the instructions provided in the T7 tag affinity purification kit (Novagen). The fractions were analyzed by SDS-PAGE, and proteins were visualized by staining with Coomassie Brilliant Blue. Fractions containing the T7-tagged fusion protein were pooled.

For purification of His-tagged octopine VirE2, *E. coli* BL21 (DE3) cells containing the expression plasmid (pE2477; see Supplemental Table 4 online) were induced with isopropyl β-D-thiogalactopyranoside and the bacterial pellet was resuspended in resuspension solution (4 M urea, 50 mM Na-phosphate buffer [pH 8], 300 mM NaCl, and 20 mM imidazole [Sigma-Aldrich]). The suspension was sonicated and then centrifuged to remove cell debris as described earlier. The supernatant solution was added to a column containing nickel-nitrilotriacetic acid agarose resin (Qiagen) previously washed with 10 bed volumes of chilled resuspension buffer. The supernatant solution was allowed to flow through, and the resin was washed with 20 bed volumes of chilled resuspension solution. Bound proteins were eluted in 1-mL fractions with chilled elution buffer (4 M urea, 50 mM Na-phosphate buffer [pH 8], 300 mM NaCl, and 250 mM imidazole). The fractions were dialyzed overnight at 4°C against a buffer containing 50 mM Na-phosphate buffer (pH 8), 300 mM NaCl, and 20% glycerol. The fractions were analyzed by SDS-PAGE, and proteins were visualized by staining with Coomassie Brilliant Blue. Fractions containing His-tagged VirE2 fusion proteins were pooled. For all protein quantification, a Bradford assay was used with BSA as standard.

The GST fusion protein was bound to glutathione–Sepharose beads as described above. As a negative control, GST alone was linked to glutathione–Sepharose beads. The protein-bound beads were washed with 20 bed volumes of chilled binding buffer (20 mM Tris-HCl [pH 7.5], 75 mM KCl, 50 mM NaCl, 1 mM EDTA [pH 8], 0.05% Nonidet P-40, 10% glycerol, 1 mM DTT, and 1 mM PMSF). *E. coli* cell lysates from cultures expressing the T7-tagged (or untagged) proteins were passed through the glutathione–Sepharose column containing the corresponding GST-tagged protein (or GST alone). The column was washed with 20 bed volumes of chilled binding buffer, and the bound proteins were eluted with 50 mM Tris-HCl [pH 8] containing 5 mM reduced glutathione. The eluted fractions were analyzed by SDS-PAGE. Eluted fraction volumes corresponding to equimolar amounts of the first protein were subjected to SDS-PAGE, and after transfer to a nitrocellulose membrane, the proteins

were subjected to protein gel blot analysis using the appropriate antibodies.

In Vitro Gel Mobility Shift Assay

A 237-bp *Arabidopsis* glyceraldehyde 3-phosphate dehydrogenase cDNA fragment obtained from the plasmid pE2565 by *Eco*RI digestion was used for the assay. The double-stranded DNA fragment was quantified, and fragment amounts equivalent to 10 pmol of 5′ ends were 5′ end labeled using [γ-^{32}P]dATP (Amersham) following the instructions in the DNA 5′ end labeling kit (Promega). The two denatured ssDNA strands had significant differences in mobility and were separated by electrophoresis at 4°C through a 4% polyacrylamide gel cast in low-ionic-strength buffer (6.7 mM Tris-HCl [pH 7.5], 1 mM EDTA, and 3.3 mM sodium acetate). The gel was prerun at a potential of 65 V for 20 min prior to loading of sample. Electrophoresis was performed at 4°C at a similar voltage for 24 h. The gel was gently transferred to a plastic wrap and exposed to x-ray film (Kodak). The x-ray film was developed and aligned to the gel. A gel slice corresponding to the more rapidly migrating ssDNA was cut, and the DNA was eluted by electrophoresis, precipitated, and resuspended in binding buffer (20 mM Tris-HCl [pH 7.5], 75 mM KCl, 50 mM NaCl, 1 mM EDTA [pH 8], 0.05% Nonidet P-40, 10% glycerol, 1 mM DTT, and 1 mM PMSF). The labeled ssDNA was quantified by measuring the A_{260}. His-tagged octopine VirE2 and T7-tagged IMPa-4 proteins were dialyzed overnight at 4°C against binding buffer.

To determine the minimal concentration of VirE2 protein required to saturate fully the ssDNA binding sites, labeled ssDNA (5 ng for each reaction) was incubated on ice for 15 min with increasing amounts of purified His-tagged octopine VirE2 protein (7 to 50 ng VirE2, 20 μL of each reaction volume). Loading solution (6 μL of 10% glycerol and 0.1% bromphenol blue) was added to the reaction mixture, and electrophoresis was performed as described above. The gel was dried and subjected to autoradiography.

To determine whether ssDNA-bound VirE2 protein interacted with importin α, labeled ssDNA was preincubated with VirE2 (5 ng of ssDNA per 30 ng of VirE2) on ice for 15 min followed by addition of increasing amounts of T7-tagged IMPa-4 protein (20 to 400 ng, 20 μL of each reaction volume). The mixture was incubated on ice for 20 min followed by the addition of loading solution. As a control, 400 ng of IMPa-4 was incubated with 5 ng of labeled ssDNA in the absence of VirE2. Electrophoresis was performed as described above. The gel was dried and subjected to autoradiography.

To investigate whether the preformed IMPa-4–VirE2 protein complex binds ssDNA, 400 ng of IMPa-4 was preincubated on ice for 15 min with 30 ng of VirE2. To this mixture, 5 ng of labeled ssDNA was added (reaction volume of 20 μL) followed by additional incubation on ice for 20 min. Loading solution was added, and electrophoresis was performed as discussed above. To identify the ssDNA–VirE2–IMPa-4 complex, a parallel lane containing ssDNA-bound VirE2 complex was used as a control (30 ng of VirE2 protein bound to 5 ng of labeled ssDNA). The negative control lane contained 400 ng of IMPa-4 preincubated with 5 ng of labeled ssDNA. The gel was dried and subjected to autoradiography.

Identification of *Arabidopsis* Lines from the Feldmann and Salk T-DNA Insertion Collection with T-DNA Insertions in the Individual Importin α Genes

A PCR-based reverse genetics approach similar to that described by Zhu et al. (2003) was used to identify an *Arabidopsis* line (ecotype Ws-2) with a T-DNA insertion in the *IMPa-4* gene. Briefly, PCR primers specific to each of the four members of the *Arabidopsis* importin α gene family were designed and used in combination with the mutagenizing T-DNA right or left border primer. T-DNA– and *IMPa-4*–specific primer sequences are presented in Supplemental Table 3 online. PCR was successively performed on genomic DNA isolated from pools of 1000, 100, and 20 T-DNA insertion lines. PCR amplification conditions were as follows: 95°C for 5 min; 36 cycles at 94°C for 40 s, 56°C for 1 min, 72°C for 3 min, 72°C for 10 min, and 4°C hold. PCR products of the expected sizes were sequenced to identify the T-DNA–plant DNA junctions. Using these approaches, the PCR product was narrowed to a single *Arabidopsis* plant. Seeds harvested from this plant were used for genotyping and RT-PCR analyses.

Seeds of *Arabidopsis* (ecotype Columbia; CS60,000) with T-DNA insertions in the importin α genes (*KAPα*, *IMPa-2*, and *IMPa-3*) were identified using the SIGnAL T-DNA Express *Arabidopsis* Gene Mapping Tool (http://signal.salk.edu/; Alonso et al., 2003) and were obtained from the ABRC at Ohio State University and subsequently used for genotyping and RT-PCR analyses.

Genotyping and RT-PCR Analyses of *Arabidopsis* Lines with T-DNA Insertions in the Individual Importin α Genes

Genomic DNA isolated from 3-week-old plants was used for PCR-based genotypic analyses. For genotyping, the *impa-4* mutant obtained from the Feldmann collection, the right border, the left border, and the *IMPa-4*–specific primers were as mentioned in Supplemental Table 3 online. For genotyping the importin α mutants obtained from the Salk collection, the primer sequences are presented in Supplemental Table 3 online. PCR products of appropriate sizes, when obtained, were sequenced to identify the T-DNA–plant DNA junctions.

For RT-PCR analysis, 2 μg of total RNA from 2- to 3-week-old plants was first reverse-transcribed using oligo(dT) primers and then PCR-amplified with importin α–specific primers using the amplification conditions described above. For *KAPα*, *IMPa-2*, and *IMPa-4*, the primers were the same as those used for the genotyping. For *IMPa-3*, the forward primer used for genotyping was used in combination with a reverse primer as presented in Supplemental Table 3 online. *Arabidopsis ACTIN2* (*ACT2*)-specific primers were used as a positive control to demonstrate equivalent efficiencies of double-stranded cDNA amplification in the samples investigated. The sequences of the *actin2* primers are presented in Supplemental Table 3 online.

Measurement of Transcript Levels by Real-Time PCR

Total RNA was isolated as described earlier (Hwang and Gelvin, 2004). A 5-μg aliquot of purified RNA was reverse-transcribed in a 20-μL reaction volume using the SuperScript II first-strand cDNA synthesis system and oligo(dT)$_{12-18}$ according to the manufacturer's instructions (Invitrogen). The reaction was terminated by heat inactivation at 70°C for 15 min. Subsequently, the reaction mix was diluted 1:25 with water, and 20 μL of the diluted cDNA (corresponding to 100 ng of total RNA) was used as a template for real-time PCR analysis with the Rotor-Gene 2000 (Corbett Research). Amplification mixtures (20 μL per reaction) consisted of 1× Ex Taq buffer (Takara Bio), 0.2 mM deoxynucleotide triphosphate, 0.2 M each primer, 1:20,000 times diluted SYBR Green I (Molecular Probes), 0.5 units of TaKaRa Ex Taq (Takara Bio), and cDNA corresponding to 100 ng of total RNA. Cycling conditions were as follows: 5 min at 94°C; 35 cycles of 20 s at 94°C, 20 s at 54°C, and 30 s at 72°C; product extension at 72°C for 5 min. This was followed by a melting-curve program (72 to 99°C, with a 5-s hold at each temperature). Fluorescence data were acquired at the 72°C step and during the melting-curve program. For the real-time PCR analysis, gene-specific primers were prepared as presented in Supplemental Table 3 online. The identities of the amplicons and the specificity of the reaction were verified by agarose gel electrophoresis, melting-curve analysis, and sequencing. Absolute and relative copy numbers of individual mRNA species were calculated with standard curves of known copy numbers for each of the importin α cDNAs. Four replicates of each sample and standard concentrations were included with every

experiment, along with no-template controls. Rotor-Gene 5.0.37 software (Corbett Research) was used to determine the optimal cycle threshold from the dilution series of standards and to calculate the mean expression level for each set of four replicates for each cDNA.

Peptide Antibody Synthesis and Protein Blot Analysis

Synthesis of an IMPa-4–specific peptide, generation of polyclonal antibodies against this peptide in rabbits, and affinity purification of the raised antibodies were performed at GenScript. In order to link the IMPa-4–specific peptide STRAELRKKIYKTG to the carrier protein KLH (for Keyhole Limpet Hemocyanin), a Cys residue was added to the C terminus of this peptide.

For protein blot analysis, plant tissue was ground to a fine powder and resuspended in 1 volume of 2× Laemmli buffer in an Eppendorf tube. Samples were incubated in boiling water for 15 min and centrifuged at 14,000 rpm at room temperature, and the supernatant solution was transferred to a new Eppendorf tube. For protein blot analysis of *E. coli* extracts, cells were pelleted and resuspended in 2× Laemmli buffer and boiled for 5 min. Proteins were separated through 10% SDS polyacrylamide gels. Proteins were either stained with Coomassie Brilliant Blue or transferred to a nitrocellulose membrane (BioTraceNT; Pall Corporation). For immunostaining, membranes were blocked in 1× TBS-T (0.05 M Tris-HCl, 150 mM NaCl, and 0.1% [v/v] Tween, pH 7.6) with 5% (w/v) skim milk for at least 1 h. After washing the membranes three times for 5 min in 1× TBS-T, the membranes were incubated for 60 min in 1× TBS-T with 0.5% skim milk and a 1:1000 dilution of the affinity-purified antibody raised against IMPa-4. Membranes were washed four times for 5 min in 1× TBS-T and incubated for 60 min in 1× TBS-T with 0.5% skim milk and the secondary antibody, a 1:10,000 dilution of goat anti-rabbit IgG horseradish peroxidase conjugate (12-348; Upstate). Membranes were washed four times for 10 min in 1× TBS-T. To visualize IMPa-4 protein, we used a SuperSignal West Femto trial kit (Pierce). Membranes were exposed to CL-Xposure film (Pierce).

Construction of *IMPa-4* RNAi Lines

We generated an RNAi construct specifically targeting *IMPa-4* as follows. We PCR-amplified a 789-bp fragment containing 79 bp of the coding sequence and 710 bp of the 3′ UTR. This region shows no significant homology to other *Arabidopsis thaliana IMPa* genes or to other *Arabidopsis* genes. We designed primers such that two restriction sites were added to each end of the PCR product: *Xba*I and *Asc*I restriction sites at the 5′ end and *Bam*HI and *Swa*I sites at the 3′ end. The primer sequences are presented in Supplemental Table 3 online. PCR was performed using DNA from the *Arabidopsis* BAC clone T12M4 (obtained from the ABRC). The PCR product was cloned into pUC19 digested with *Hin*cII, the sequence was verified, and the construction was designated pE3201. The RNAi construct was made according to the instructions at www.chromdb.org. First, a *Swa*I/*Asc*I fragment from pE3201 was cloned into the RNAi vector pFGC5941 (Kerschen et al., 2004) digested with the same enzymes, then a *Xba*I/*Bam*HI fragment from pE3201 was cloned into the previous construct digested with *Xba*I/*Bam*HI. This final construct was transformed into *Agrobacterium tumefaciens* GV3101 (Koncz and Schell, 1986). *Arabidopsis* plants (ecotypes Ws-2 and Columbia) were transformed by a floral dip protocol (Clough and Bent, 1998). Transgenic plants were selected on B5 medium supplemented with 100 μg/mL timentin and 10 μg/mL phosphinothricin.

Construction of Binary Vectors and Generation of Importin α cDNA Overexpression Lines in the *impa-4* Mutant Background

The *KAP*α, *IMPa-2*, *IMPa-3*, or *IMPa-4* cDNAs were cloned as *Xba*I/*Hin*cII fragments into the *Xba*I-T4 polymerase–filled *Sac*I sites of pE1546, a T-DNA binary vector with a CaMV 35S promoter, to express the cDNAs and a *hptII* gene as the plant selectable marker. The cDNA of *IMPa-6* was cloned as a *Sal*I/*Sac*I fragment into pE1546 digested with the same enzymes. The cDNA of *IMPa-7* was cloned as a *Sal*I/*Eco*RI Klenow filled-in fragment into pE1546 digested with *Sal*I and filled in using Klenow. The cDNA of *IMPa-9* was cloned as a *Bam*HI Klenow-filled fragment into pE1546 digested with *Sal*I and filled in using Klenow. These various binary vectors were introduced into the disarmed *Agrobacterium* strain GV3101 (Koncz and Schell, 1986), and the resulting *Agrobacterium* strains were used to generate transgenic *Arabidopsis* plants in the *impa-4* mutant background using a floral dip transformation protocol (Clough and Bent, 1998).

Construction of Binary Vectors and Generation of Transgenic Plants Expressing YFP-Tagged VirD2 and VirE2

For the binary vector expressing a YFP-VirD2 fusion protein, the C-terminal *Nru*I fragment (~135 bp) of octopine VirD2 was fused in the correct reading frame downstream of the EYFP gene at the *Sma*I site of pCAM-35S-EYFP-C1 (a kind gift from Erik Nielsen at the Donald Danforth Plant Science Center), resulting in the plasmid pE2837. For the binary vectors expressing YFP-VirE2 or VirE2-YFP, the corresponding YFP-VirE2 or VirE2-YFP fusion sequences, obtained as a *Nco*I/*Xba*I fragment from pE2774 or pE2775, respectively, were individually subcloned into the *Nco*I–*Xba*I sites of pCAM-35S-EYFP-C1 to generate pE2838 or pE2836, respectively. A polylinker sequence (5′-GAGAGGAAAGA-GAGG-3′) separates the two fusion proteins in YFP-VirE2 or VirE2-YFP. The above binary vectors along with a control vector, pCAM-35S-EYFP-C1 (pE2829), were used to generate transgenic plants in the wild type and in the *impa-4* mutant background utilizing the *Agrobacterium*-mediated floral dip transformation protocol as described above.

BiFC

Genes encoding VirD2 and VirE2 from pTiA6 were cloned into the various BiFC vectors pSAT6-nEYFP-C1, pSAT6-nEYFP-N1, and pSAT6-cEYFP-N1 (Citovsky et al., 2006). *virD2* was cloned as an *Eco*RI/*Sac*II fragment, and *virE2* was cloned as a *Nco*I/*Bam*HI fragment. cDNAs (lacking translation stop codons) of *KAP*α, *IMPa-4*, *IMPa-7*, and *IMPa-9* were cloned into the BiFC vectors pSAT6-nEYFP-N1 and pSAT6-cEYFP-N1 as *Nco*I/*Xma*I fragments. For multicolor BiFC, proteins were tagged with cCFP (amino acids 155 to 239), nVenus (amino acids 1 to 174), or nCerulean (amino acids 1 to 174) as described (Shyu et al., 2006). In some instances, mRFP (for red fluoresecent protein; Campbell et al., 2002) or mCherry (Shaner et al., 2004) was coexpressed from a CaMV double 35S promoter (Restrepo et al., 1990). Tobacco (*Nicotiana tabacum*) BY-2 protoplasts were prepared and coelectroporated with 20 μg of each BiFC construction as described previously (Mysore et al., 1998). In some instances, the cells were stained with 2 μg/mL Hoechst 33242 (Molecular Probes) in PBS–0.4 M mannitol buffer, and fluorescence was visualized using a Nikon Eclipse E600 fluorescence microscope.

We generated IMPa-4–nYFP and –cYFP constructions within the native context of the gene as follows. We cloned a 6351-bp *Hin*cII fragment, harboring the *IMPa-4* gene, from BAC clone T12M4 into pUC19 digested with *Hin*cII and designated this clone pE3203. This *Hin*cII fragment contains 2257 bp upstream of the putative translational start codon, the entire coding region of the *IMPa-4* gene (exons and introns), and 766 bp downstream of the stop codon. This construction is flanked by two *Sal*I sites. To enable generation of in-frame fusions, we digested pSat6-n(1-174)EYFP-N1 and pSat6-c(175-end)EYPF-N1 (Tzfira et al., 2005) with *Xma*I and filled in the overhanging ends using Klenow fragment of DNA polymerase, then digested the vectors with *Xho*I. We subcloned a *Xho*I/*Msp*A1I fragment, containing the 3′ end of the *IMPa-4* coding sequence, into the digested pSat vectors and partially sequenced them to confirm that the *IMPa-4* open reading frames were in-frame with the YFP fragments. These clones were designated pE3204 (nYPF-tagged *IMPa-4*

fragment) and pE3205 (cYPF-tagged *IMPa-4* fragment). We next used PCR to amplify a 612-bp fragment harboring the 3′ UTR and the putative terminator region of IMPa-4, using the primers presented in Supplemental Table 3 online. This amplification added a *Xba*I site to the 5′ end and a *Not*I site to the 3′ end of the PCR product. The PCR product was first cloned into pBluescript KS+ digested with *Sma*I, then the *Xba*I/*Not*I fragment of this clone was ligated into both pE3204 and pE3205 digested with the same enzymes. Finally, we individually cloned *Xho*I/*Cla*I fragments from pE3204 and pE3205 into pE3203 that was digested with the same enzymes. The resulting constructs were designated pE3292 (nYPF-tagged *IMPa-4*) and pE3293 (cYPF-tagged *IMPa-4*). *Sal*I fragments from pE3203, pE3292, and pE3293 were ligated into the T-DNA binary vector pCAMBIA1300 cut with the same enzyme, and the constructs were transformed into *Agrobacterium* GV3101 and EHA105 by electroporation (Nagel et al., 1990).

Agrobacterium-Mediated Transient and Stable Transformation Assays

All *Agrobacterium* strains were cultured in 5 mL of yeast extract peptone (Lichenstein and Draper, 1986) supplemented with the appropriate antibiotics (rifampicin, 10 μg/mL; kanamycin, 25 μg/mL) at 30°C. Two milliliters of an overnight bacterial culture was inoculated into 25 mL of YEP medium with appropriate antibiotics and grown at 30°C to an A_{600} of 0.85 (1 to 2×10^9 cells/mL). The cells were washed with sterile 0.9% NaCl and resuspended in 0.9% NaCl at 2×10^8 cells/mL for stable and transient root transformation assays.

Seeds from the wild type and from the various transgenic plants generated were surface-sterilized with a solution containing 50% commercial bleach and 0.1% SDS for 10 min and rinsed five times with sterile distilled water. Seeds were resuspended in sterile distilled water and incubated in the dark at 4°C for 2 d. Seeds were then placed on Gamborg's B5 medium (GIBCO) containing 0.75% Bactoagar (BD Biosciences) and appropriate antibiotics (timentin, 100 μg/mL; kanamycin, 50 μg/mL for the T-DNA mutants; hygromycin, 20 μg/mL for the various importin α overexpression lines or the YFP, YFP-VirD2, YFP-VirE2, and VirE2-YFP overexpression lines). Wild-type seeds were placed on medium lacking the antibiotics. The plates were incubated for 10 d under a 16-h-light/8-h-dark photoperiod at 25°C. Seedlings were transferred individually into baby food jars containing solidified B5 medium without any antibiotics, grown for 3 weeks, and then used for transformation assays as described by Nam et al. (1997, 1998, 1999) and Zhu et al. (2003).

For transient transformation assays, infection was performed with *Agrobacterium* GV3101 (Koncz and Schell, 1986) containing the binary vector pBISN1 (Narasimhulu et al., 1996) as described (Nam et al., 1997, 1998, 1999; Zhu et al., 2003). pBISN1 contains within the T-DNA a *gusA* intron gene under the control of a superpromoter (Narasimhulu et al., 1996). Transient transformation efficiency was reported as the percentage of root segments showing GUS staining.

For stable transformation assays, the tumorigenic strain *Agrobacterium* A208 was used. After a 2-d cocultivation period, root bundles were separated into single root segments onto Murashige and Skoog basal medium plates containing 100 μg/mL timentin. The plates were incubated at 23°C for 4 weeks, after which they were scored for tumor development and the tumors were categorized according to morphology (large green, small green, large yellow, or small yellow). Stable transformation efficiency was reported as the percentage of total root segments showing tumors.

Confocal Microscopy Analyses of the YFP-Expressing *Arabidopsis* Lines

Several independent 1-week-old transgenic T1 plants expressing either YFP or YFP-Vir protein fusions were placed on their sides on B5 agar plates containing appropriate antibiotics (timentin, 100 μg/mL; hygromycin, 20 μg/mL) and grown in a vertical position for an additional 2 weeks. Root segments (2 to 3 mm) containing the tip meristematic regions were excised and immediately fixed for 1 h at room temperature with fixative solution (4% [v/v] paraformaldehyde [Sigma-Aldrich], 0.2% Nonidet P-40 in PEM 50:5:5 [pH 5.7]). PEM 50:5:5 contains 50 mM PIPES, 5 mM EGTA, and 5 mM $MgSO_4$. The root segments were washed twice for 5 min each with PEM 50:5:5 and then counterstained for 15 min with Hoechst 33242 (2 μg/mL). After an additional wash for 5 min with PEM 50:5:5, the root segments were mounted on slides containing a drop of fluorescent mounting medium (0.1 M Tris-HCl [pH 9.0], 50% glycerol, and 1 mg/mL *p*-phenylenediamine hydrochloride [Sigma-Aldrich]). Confocal microscopy analysis was performed using the Bio-Rad Radiance 2100 MP rainbow system microscope equipped with 20× multi-immersion and 60× water objectives.

Accession Numbers

Sequence data from this article can be found in the Arabidopsis Genome Initiative or GenBank/EMBL databases under the following accession numbers: *KAPα*, At3g06720; *IMPa-2*, At4g16143; *IMPa-3*, At4g02150; *IMPa-4*, At1g09270; *IMPa-5*, At5g49310; *IMPa-6*, At1g02690; *IMPa-7*, At3g05720; *IMPa-8*, At5g52000; *IMPa-9*, At5g03070; *ACT2*, At3g18780; *UBQ5*, At3g62250.

Supplemental Data

The following materials are available in the online version of this article.

Supplemental Figure 1. Amino Acid Alignment of the Seven Importin α Proteins Investigated.

Supplemental Figure 2. Importin α–Interacting Domains of VirD2 and VirE2 Are Not Restricted to NLS Residues.

Supplemental Figure 3. Saturation Kinetics of ssDNA Binding Activity by VirE2.

Supplemental Figure 4. Homozygous *Arabidopsis* Importin α Mutants Show Reduction in the Corresponding Importin α Transcripts.

Supplemental Figure 5. Peptide Antibody against *Arabidopsis* IMPa-4 Detects Recombinant IMPa-4 but Not IMPa-1, -2, or -3.

Supplemental Figure 6. Expression of Various Importin α Transcripts in Tissues of Wild-Type Plants.

Supplemental Figure 7. VirE2-YFP Localizes to the Cytoplasm of Electroporated Tobacco BY-2 Cells.

Supplemental Table 1A. Stable and Transient Transformation Assays on T2 Lines Overexpressing Various Importin α Isoforms in the *impa-4* Mutant Background.

Supplemental Table 1B. Stable Transformation Assays on T1 Lines Overexpressing Various Importin α Isoforms in the *impa-4* Mutant Background.

Supplemental Table 2. Localization of BiFC Signal in Electroporated Tobacco BY-2 Cells.

Supplemental Table 3. Primers Used in PCR.

Supplemental Table 4. Plasmids Used in Yeast Two-Hybrid, in Vitro, and in Planta Interaction Assays.

Supplemental Data Set 1. Sequences Used to Generate the Cladogram in Figure 1.

ACKNOWLEDGMENTS

We thank Vitaly Citovsky (State University of New York, Stony Brook) and Natasha Raikhel (University of California, Riverside) for kindly

providing anti-VirE2 and anti-KAPα polyclonal antibodies, respectively; Vitaly Citovsky for providing the yeast strain CTY10-5d; and Tzvi Tzfira for providing BiFC vectors. We thank Jenny Sturgis at the Purdue University Cytometry Laboratories for help with confocal microscopy analysis and Joerg Spantzel for help with the transformation assays. This work was funded by grants from the National Science Foundation Plant Genome (Grant 99-75715) and Arabidopsis 2010 (Grant MCB-0418709) programs, the U.S. Department of Agriculture (Grant 2001-35304-10891), the Biotechnology Research and Development Corporation, and the Corporation for Plant Biotechnology Research. We also acknowledge support from the Purdue University Cancer Center (P30 grant).

Received May 9, 2008; revised August 15, 2008; accepted September 15, 2008; published October 3, 2008.

REFERENCES

Alonso, J.M., et al. (2003). Genome-wide insertional mutagenesis of *Arabidopsis thaliana*. Science **301:** 653–657.

Ausubel, F.M., Brent, R., Kingston, R.E., More, D.D., Seidman, J.G., Smith, J.A., and Struhl, K. (2003). Current Protocols in Molecular Biology. (New York: John Wiley & Sons).

Bako, L., Umeda, M., Tiburcio, A.F., Schell, J., and Koncz, C. (2003). The VirD2 pilot protein of *Agrobacterium*-transferred DNA interacts with the TATA box-binding protein and a nuclear protein kinase in plants. Proc. Natl. Acad. Sci. USA **100:** 10108–10113.

Ballas, N., and Citovsky, V. (1997). Nuclear localization signal binding proteins from *Arabidopsis* mediates nuclear import of *Agrobacterium* VirD2 protein. Proc. Natl. Acad. Sci. USA **94:** 10723–10728.

Becker, D.M., and Lundblad, V. (1994). Basic techniques of yeast genetics. In Current Protocols in Molecular Biology, Vol. 2, F.M. Ausubel, R. Brent, R.E. Kingston, D.D. Moore, J.G. Seidman, J.A. Smith, and K. Struhl, eds (New York: John Wiley & Sons), pp. 13.7.1–13.7.2.

Bednenko, J., Cingolani, G., and Gerace, L. (2003). Importin β contains a COOH-terminal nucleoporin binding region important for nuclear transport. J. Cell Biol. **162:** 391–401.

Binns, A.N., Beaupré, C.F., and Dale, E.M. (1995). Inhibition of VirB-mediated transfer of diverse substrates from *Agrobacterium tumefaciens* by the IncQ plasmid RSF1010. J. Bacteriol. **177:** 4890–4899.

Campbell, R.E., Tour, O., Palmer, A.E., Steinbach, P.A., Baird, G.S., Zacharias, D.A., and Tsien, R.Y. (2002). A monomeric red fluorescent protein. Proc. Natl. Acad. Sci. USA **99:** 7877–7882.

Citovsky, V., Guralnick, B., Simon, M.N., and Wall, J.S. (1997). The molecular structure of *Agrobacterium* VirE2-single stranded DNA complexes involved in nuclear import. J. Mol. Biol. **271:** 718–727.

Citovsky, V., Lee, L.-Y., Vyas, S., Glick, E., Chen, M.-H., Vainstein, A., Gafni, Y., Gelvin, S.B., and Tzfira, T. (2006). Subcellular localization of interacting proteins by bimolecular fluorescence complementation *in planta*. J. Mol. Biol. **362:** 1120–1131.

Citovsky, V., Warnick, D., and Zambryski, P. (1994). Nuclear import of *Agrobacterium* VirD2 and VirE2 proteins in maize and tobacco. Proc. Natl. Acad. Sci. USA **91:** 3210–3214.

Citovsky, V., Wong, M.L., and Zambryski, P. (1989). Cooperative interaction of *Agrobacterium* VirE2 protein with single-stranded DNA: Implications for the T-DNA transfer process. Proc. Natl. Acad. Sci. USA **86:** 1193–1197.

Citovsky, V., Zupan, J., Warnick, D., and Zambryski, P. (1992). Nuclear localization of *Agrobacterium* VirE2 protein in plant cells. Science **256:** 1802–1805.

Clough, S.J., and Bent, A.F. (1998). Floral dip: A simplified method for *Agrobacterium*-mediated transformation of *Arabidopsis thaliana*. Plant J. **16:** 735–743.

Dombek, P., and Ream, W. (1997). Functional domains of *Agrobacterium tumefaciens* single-stranded DNA-binding protein VirE2. J. Bacteriol. **179:** 1165–1173.

Duckely, M., and Hohn, B. (2003). The VirE2 protein of *Agrobacterium tumefaciens*: The Yin and Yang of T-DNA transfer. FEMS Microbiol. Lett. **223:** 1–6.

Duckely, M., Oomen, C., Axthelm, F., Van Gelder, P., Waksman, G., and Engel, A. (2005). The VirE1VirE2 complex of *Agrobacterium tumefaciens* interacts with single-stranded DNA and forms channels. Mol. Microbiol. **58:** 1130–1142.

Dumas, F., Duckely, M., Pelczar, P., Van Gelder, P., and Hohn, B. (2001). An *Agrobacterium* VirE2 channel for transferred-DNA transport into plant cells. Proc. Natl. Acad. Sci. USA **98:** 485–490.

Durrenberger, F., Crameri, A., Hohn, B., and Koukolikova-Nicola, Z. (1989). Covalently bound VirD2 protein of *Agrobacterium tumefaciens* protects the T-DNA from exonucleolytic degradation. Proc. Natl. Acad. Sci. USA **86:** 9154–9158.

Filichkin, S.A., and Gelvin, S.B. (1993). Formation of a putative relaxation intermediate during T-DNA processing directed by the *Agrobacterium tumefaciens* VirD1, D2 endonuclease. Mol. Microbiol. **8:** 915–926.

Gasiorowski, J.Z., and Dean, D.A. (2003). Mechanisms of nuclear transport and interventions. Adv. Drug Deliv. Rev. **55:** 703–716.

Gelvin, S.B. (1998). *Agrobacterium* VirE2 proteins can form a complex with T strands in the plant cytoplasm. J. Bacteriol. **180:** 4300–4302.

Gelvin, S.B. (2000). *Agrobacterium* and plant proteins involved in T-DNA transfer and integration. Annu. Rev. Plant Physiol. Plant Mol. Biol. **51:** 223–256.

Gelvin, S.B. (2003). *Agrobacterium*-mediated plant transformation: The biology behind the 'gene-jockeying' tool. Microbiol. Mol. Biol. Rev. **67:** 16–37.

Goldfarb, D.S., Corbett, A.H., Mason, D.A., Harreman, M.T., and Adam, S.A. (2004). Importin alpha: A multipurpose nuclear-transport receptor. Trends Cell Biol. **14:** 505–514.

Görlich, D., Kostka, S., Kraft, R., Dingwall, C., Laskey, S.A., Hartmann, E., and Prehn, S. (1995). Two different subunits of importin cooperate to recognize nuclear localization signal and bind them to the nuclear envelope. Curr. Biol. **5:** 383–392.

Grange, W., Duckely, M., Husale, S., Jacob, S., Engel, A., and Hegner, M. (2008). VirE2: A unique ssDNA-compacting molecular machine. PLoS Biol. **6:** 343–351.

Guralnick, B., Thomsen, G., and Citovsky, V. (1996). Transport of DNA into the nuclei of *Xenopus* oocytes by a modified VirE2 protein of *Agrobacterium*. Plant Cell **8:** 363–373.

Herrera-Estrella, A., Chen, Z.-M., Van Montagu, M., and Wang, K. (1988). VirD proteins of *Agrobacterium tumefaciens* are required for the formation of a covalent DNA-protein complex at the 5′ terminus of T-strand molecules. EMBO J. **7:** 4055–4062.

Herrera-Estrella, A., Van Montagu, M., and Wang, K. (1990). A bacterial peptide acting as a plant nuclear targeting signal: The amino terminal portion of *Agrobacterium* VirD2 protein directs β-galactosidase fusion protein into tobacco nuclei. Proc. Natl. Acad. Sci. USA **87:** 9534–9537.

Howard, E.A., Zupan, J.R., Citovsky, V., and Zambryski, P.C. (1992). The VirD2 protein of *A. tumefaciens* contains a C-terminal bipartite nuclear localization signal: Implications for nuclear uptake of DNA in plant cells. Cell **68:** 109–118.

Hu, C.-D., Chinenov, Y., and Kerppola, T.K. (2002). Visualization of interactions among bZIP and Rel family proteins in living cells using bimolecular fluorescence complementation. Mol. Cell **9:** 789–798.

Hu, C.-D., and Kerppola, T.K. (2003). Simultaneous visualization of multiple protein interactions in living cells using multicolor fluorescence complementation analysis. Nat. Biotechnol. **21:** 539–545.

Hwang, H.-H., and Gelvin, S.B. (2004). Plant proteins that interact with VirB2, the *Agrobacterium* pilin protein, are required for plant transformation. Plant Cell **16:** 3148–3167.

Hwang, H.-H., Mysore, K.S., and Gelvin, S.B. (2006). Transgenic *Arabidopsis* plants expressing *Agrobacterium tumefaciens* VirD2 protein are less susceptible to *Agrobacterium* transformation. Mol. Plant Pathol. **6:** 743–754.

Jayaswal, R.K., Veluthambi, K., Gelvin, S.B., and Slightom, J.L. (1987). Double-stranded cleavage of T-DNA and generation of single-stranded T-DNA molecules in *Escherichia coli* by a *virD*-encoded border-specific endonuclease from *Agrobacterium tumefaciens.* J. Bacteriol. **169:** 5035–5045.

Kerschen, A., Napoli, C.A., Jorgensen, R.A., and Müller, A.E. (2004). Effectiveness of RNA interference in transgenic plants. FEBS Lett. **566:** 223–228.

Köhler, M., Ansieau, S., Prelin, S., Leutz, A., Haller, H., and Hartmann, E. (1997). Cloning of two novel importin-α subunits and analysis of the expression pattern of the importin-α protein family. FEBS Lett. **417:** 104–108.

Koncz, C., and Schell, J. (1986). The promoter of TL-DNA gene 5 controls the tissue-specific expression of chimaeric genes carried by a novel type of *Agrobacterium* binary vector. Mol. Gen. Genet. **204:** 383–396.

Lacroix, B., Tzfira, T., Vainstein, A., and Citovsky, V. (2006). A case of promiscuity: *Agrobacterium's* endless hunt for new partners. Trends Genet. **22:** 29–37.

Lee, L.-Y., Gelvin, S.B., and Kado, C.I. (1999). pSa causes oncogenic suppression of *Agrobacterium* by inhibiting VirE2 protein export. J. Bacteriol. **181:** 186–196.

Li, J., Krichevsky, A., Vaidya, M., Tzfira, T., and Citovsky, V. (2005). Uncoupling of the functions of the *Arabidopsis* VIP1 protein in transient and stable plant genetic transformation by *Agrobacterium*. Proc. Natl. Acad. Sci. USA **102:** 5733–5738.

Lichenstein, C., and Draper, J. (1986). Genetic engineering of plants. In DNA Cloning: A Practical Approach, Vol. 2, D.M. Glover and B.D. Hames, eds (Oxford, UK: IRL Press), pp. 67–119.

Mason, D.A., Fleming, R.J., and Goldfarb, D.S. (2002). *Drosophila melanogaster* importin α1 and α3 can replace importin α2 during spermatogenesis but not oogenesis. Genetics **161:** 157–170.

McCullen, C.A., and Binns, A.N. (2006). *Agrobacterium tumefaciens* and plant cell interactions and activities required for interkingdom macromolecular transfer. Annu. Rev. Cell Dev. Biol. **22:** 101–127.

Mysore, K.S., Bassuner, B., Deng, X.-b., Darbinian, N.S., Motchoulski, A., Ream, W., and Gelvin, S.B. (1998). Role of the *Agrobacterium tumefaciens* VirD2 protein in T-DNA transfer and integration. Mol. Plant Microbe Interact. **11:** 668–683.

Nagel, R., Elliot, A., Masel, A., Birch, R.G., and Manners, J.M. (1990). Electroporation of binary Ti plasmid vector into *Agrobacterium tumefaciens* and *Agrobacterium rhizogenes*. FEMS Microbiol. Lett. **67:** 325–328.

Nam, J., Matthysse, A.G., and Gelvin, S.B. (1997). Differences in susceptibility of *Arabidopsis* ecotypes to crown gall disease may result from a deficiency in T-DNA integration. Plant Cell **9:** 317–333.

Nam, J., Mysore, K.S., and Gelvin, S.B. (1998). *Agrobacterium tumefaciens* transformation of the radiation hypersensitive *Arabidopsis thaliana* mutants *uvh1* and *rad5*. Mol. Plant Microbe Interact. **11:** 1136–1141.

Nam, J., Mysore, K.S., Zheng, C., Knue, M.K., Matthysse, A.G., and Gelvin, S.B. (1999). Identification of T-DNA tagged *Arabidopsis* mutants that are resistant to transformation by *Agrobacterium*. Mol. Gen. Genet. **261:** 429–438.

Narasimhulu, S.B., Deng, X.-b., Sarria, R., and Gelvin, S.B. (1996). Early transcription of *Agrobacterium* T-DNA genes in tobacco and maize. Plant Cell **8:** 873–886.

Neumann, G., Castrucci, M.R., and Kawaoka, Y. (1997). Nuclear import and export of influenza virus nucleoprotein. J. Virol. **71:** 9690–9700.

Otten, L., DeGreve, H., Leemans, J., Hain, R., Hooykaas, P., and Schell, J. (1984). Restoration of virulence of *vir* region mutants of *Agrobacterium tumefaciens* strain B6S3 by coinfection with normal and mutant *Agrobacterium* strains. Mol. Gen. Genet. **195:** 159–163.

Quimby, B.B., and Corbett, A.H. (2001). Nuclear transport mechanisms. Cell. Mol. Life Sci. **58:** 1766–1773.

Restrepo, M.A., Freed, D.D., and Carrington, J.C. (1990). Nuclear transport of plant potyviral proteins. Plant Cell **2:** 987–998.

Robbins, J., Dilworth, S.M., Laskey, R.A., and Dingwall, C. (1991). Two interdependent basic domains in nucleoplasmin nuclear targeting sequence: Identification of a class of bipartite nuclear targeting sequences. Cell **64:** 615–623.

Rossi, L., Hohn, B., and Tinland, B. (1993). The VirD2 protein of *Agrobacterium tumefaciens* carries nuclear localization signals important for transfer of T-DNA to plants. Mol. Gen. Genet. **239:** 345–353.

Rossi, L., Hohn, B., and Tinland, B. (1996). Integration of complete transferred DNA units is dependent on the activity of virulence E2 protein of *Agrobacterium tumefaciens*. Proc. Natl. Acad. Sci. USA **93:** 126–130.

Sen, P., Pazour, G.J., Anderson, D., and Das, A. (1989). Cooperative binding of *Agrobacterium tumefaciens* VirE2 protein to single-stranded DNA. J. Bacteriol. **171:** 2573–2580.

Shaner, N.C., Campbell, R.E., Steinbach, P.A., Giepmans, B.N.G., Palmer, A.E., and Tsien, R.Y. (2004). Improved monomeric red, orange and yellow fluorescent proteins derived from *Discosoma* sp. red fluorescent protein. Nat. Biotechnol. **22:** 1567–1572.

Shurvinton, C.E., Hodges, L., and Ream, W. (1992). A nuclear localization signal and the C-terminal omega sequence in the *Agrobacterium tumefaciens* VirD2 endonuclease are important for tumor formation. Proc. Natl. Acad. Sci. USA **89:** 11837–11841.

Shyu, Y.J., Liu, H., Deng, X., and Hu, C.-D. (2006). Identification of new fluorescent protein fragments for bimolecular fluorescence complementation analysis under physiological conditions. Biotechniques **40:** 61–66.

Simone, M., McCullen, C.A., Stahl, L., and Binns, A.A. (2001). The carboxy-terminus of VirE2 from *Agrobacterium tumefaciens* is required for its transport to host cells by the *virB*-encoded type IV transport system. Mol. Microbiol. **41:** 1283–1293.

Stachel, S.E., Timmerman, B., and Zambryski, P. (1986). Generation of single-stranded T-DNA molecules during the initial stages of T-DNA transfer from *Agrobacterium tumefaciens* to plant cells. Nature **322:** 706–712.

Stahl, L.E., Jacobs, A., and Binns, A.N. (1998). The conjugal intermediate of plasmid RSF1010 inhibits *Agrobacterium tumefaciens* virulence and VirB-dependent export of VirE2. J. Bacteriol. **180:** 3933–3939.

Stewart, C.L., Roux, K.J., and Burke, B. (2007). Blurring the boundary: The nuclear envelope extends its reach. Science **318:** 1408–1412.

Terry, L.J., Shows, E.B., and Wente, S.R. (2007). Crossing the nuclear envelope: Hierarchical regulation of nucleocytoplasmic transport. Science **318:** 1412–1416.

Tinland, B., Koukolíková-Nicola, Z., Hall, M.N., and Hohn, B. (1992). The T-DNA linked VirD2 contains two distinct functional nuclear localization signals. Proc. Natl. Acad. Sci. USA **89:** 7442–7446.

Tzfira, T., and Citovsky, V. (2001). Partners-in-infection: Host proteins involved in the transformation of plant cells by *Agrobacterium*. Trends Cell Biol. **12:** 121–128.

Tzfira, T., Tian, G.W., Lacroix, B.T., Vyas, S., Li, J., Leitner-Dagan, Y., Krichevsky, A., Taylor, T., Vainstein, A., and Citovsky, V. (2005). pSAT vectors: A modular series of plasmids for fluorescent protein tagging and expression of multiple genes in plants. Plant Mol. Biol. **57:** 503–516.

Tzfira, T., Vaidya, M., and Citovsky, V. (2001). VIP1, an *Arabidopsis* protein that interacts with *Agrobacterium* VirE2, is involved in VirE2 nuclear import and *Agrobacterium* infectivity. EMBO J. **20:** 3596–3607.

Tzfira, T., Vaidya, M., and Citovsky, V. (2002). Increasing plant susceptibility to *Agrobacterium* infection by overexpression of the *Arabidopsis* nuclear protein VIP1. Proc. Natl. Acad. Sci. USA **99:** 10435–10440.

Vergunst, A.C., Schrammeijer, B., den Dulk-Ras, A., de Vlaam, C.M.T., Regensburg-Tuink, T.J.G., and Hooykaas, P.J.J. (2000). VirB/D4-dependent protein translocation from *Agrobacterium* into plant cells. Science **290:** 979–982.

Vogel, A.M., and Das, A. (1992). Mutational analysis of *Agrobacterium tumefaciens virD2*: Tyrosine 29 is essential for endonuclease activity. J. Bacteriol. **174:** 303–308.

Wang, K., Stachel, S.E., Timmerman, B., Van Montagu, M., and Zambryski, P.C. (1987). Site-specific nick in the T-DNA border sequence as a result of *Agrobacterium vir* gene expression. Science **235:** 587–591.

Wang, P., Palese, P., and O'Neill, R.E. (1997). The NPI-1/NPI-3 (karyopherin alpha) binding site on the influenza a virus nucleoprotein NP is a non-conventional nuclear localization signal. J. Virol. **71:** 1850–1856.

Ward, E.R., and Barnes, W.M. (1988). VirD2 protein of *Agrobacterium tumefaciens* very tightly linked to the 5′ end of the T-strand DNA. Science **242:** 927–930.

Yanofsky, M.F., Porter, S.G., Young, C., Albright, L.M., Gordon, M.P., and Nester, E.W. (1986). The *virD* operon of *Agrobacterium tumefaciens* encodes a site-specific endonuclease. Cell **47:** 471–477.

Yi, H., Sardesai, N., Fujinuma, T., Chan, C.-W., Veena, and Gelvin, S.B. (2006). Constitutive expression exposes functional redundancy between the *Arabidopsis* histone H2A gene *HTA1* and other H2A gene family members. Plant Cell **18:** 1575–1589.

Yi, H.C., Mysore, K.S., and Gelvin, S.B. (2002). Expression of the *Arabidopsis* histone *H2A-1* gene correlates with susceptibility to *Agrobacterium* transformation. Plant J. **32:** 285–298.

Yusibov, V.M., Steck, T.R., Gupta, V., and Gelvin, S.B. (1994). Association of single-stranded transferred DNA from *Agrobacterium tumefaciens* with tobacco cells. Proc. Natl. Acad. Sci. USA **91:** 2994–2998.

Zhou, X.-R., and Christie, P.J. (1999). Mutagenesis of the *Agrobacterium* VirE2 single-stranded DNA-binding protein identifies regions required for self-association and interaction with VirE1 and a permissive site for hybrid protein construction. J. Bacteriol. **181:** 4342–4352.

Zhu, Y., et al. (2003). Identification of Arabidopsis rat mutants. Plant Physiol. **132:** 494–505.

Ziemienowicz, A., Merkle, T., Schoumacher, F., Hohn, B., and Rossi, L. (2001). Import of *Agrobacterium* T-DNA into plant nuclei: Two distinct functions of VirD2 and VirE2 proteins. Plant Cell **13:** 369–383.

Zupan, J.R., Citovsky, V., and Zambryski, P. (1996). *Agrobacterium* VirE2 protein mediates nuclear uptake of single-stranded DNA into plant cells. Proc. Natl. Acad. Sci. USA **96:** 2392–2397.

Zupan, J., Muth, T.R., Draper, O., and Zambryski, P. (2000). The transfer of DNA from *Agrobacterium tumefaciens* into plants: A feast of fundamental insights. Plant J. **23:** 11–28.